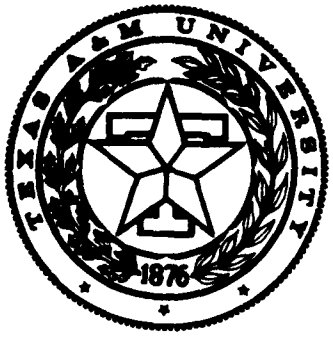

Mechanics and Materials Center
TEXAS A&M UNIVERSITY
College Station, Texas

(2)

AFOSR-TR- 88-1312

A DAMAGE MODEL FOR UNIAXIALLY REINFORCED COMPOSITES

Y. WEITSMAN AND K. LEE

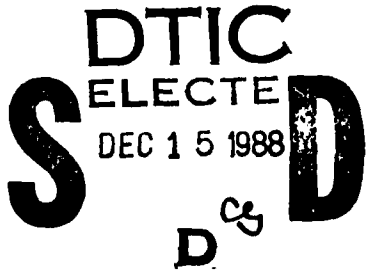

FINAL SCIENTIFIC REPORT

MARCH 1, 87 TO AUG 31, 87

AIR FORCE OFFICE OF SCIENTIFIC RESEARCH
OFFICE OF AEROSPACE RESEARCH
UNITED STATES AIR FORCE
GRANT NO. AFOSR-87-0128

M M 5662-88-9

AUGUST 1988

unclassified

SECURITY CLASSIFICATION OF THIS PAGE

REPORT DOCUMENTATION PAGE

1a. REPORT SECURITY CLASSIFICATION: unclassified	1b. RESTRICTIVE MARKINGS
2a. SECURITY CLASSIFICATION AUTHORITY	3. DISTRIBUTION/AVAILABILITY OF REPORT: Approved for public release, distribution unlimited
2b. DECLASSIFICATION/DOWNGRADING SCHEDULE	
4. PERFORMING ORGANIZATION REPORT NUMBER(S): MM-5662-88-9	5. MONITORING ORGANIZATION REPORT NUMBER(S): AFOSR-TR- 88-1312
6a. NAME OF PERFORMING ORGANIZATION: Mechanics & Materials Center, Texas A&M University; 6b. OFFICE SYMBOL (If applicable)	7a. NAME OF MONITORING ORGANIZATION: AFOSR
6c. ADDRESS (City, State and ZIP Code): College Station, Texas 77843	7b. ADDRESS (City, State and ZIP Code): Building 410, Bolling AFB, D.C. 20332-6448
8a. NAME OF FUNDING/SPONSORING ORGANIZATION: AFOSR; 8b. OFFICE SYMBOL (If applicable): NA	9. PROCUREMENT INSTRUMENT IDENTIFICATION NUMBER: Grant AFOSR-87-0128
8c. ADDRESS (City, State and ZIP Code): Building 410, Bolling AFB, D.C. 20332-6448	10. SOURCE OF FUNDING NOS. — PROGRAM ELEMENT NO.: 61102F; PROJECT NO.: 2302; TASK NO.: B2; WORK UNIT NO.:
11. TITLE (Include Security Classification): A Damage Model for Uniaxially Reinforced Composites	
12. PERSONAL AUTHOR(S): Y. Weitsman and K. Lee	
13a. TYPE OF REPORT: Final Scientific; 13b. TIME COVERED: FROM 3/1/87 TO 8/31/87	14. DATE OF REPORT (Yr., Mo., Day): August 1988; 15. PAGE COUNT: 39
16. SUPPLEMENTARY NOTATION	
17. COSATI CODES — FIELD / GROUP / SUB. GR.	18. SUBJECT TERMS (Continue on reverse if necessary and identify by block number): Continuum Damage Theory. Composite Materials. Coupled Heat Conduction. (JES)

19. ABSTRACT (Continue on reverse if necessary and identify by block number)

This report concerns a continuum damage model for uni-directionally reinforced composites that contain a multitude of micro cracks. Consideration is given to the coupling between mechanical and thermal effects. Damage is introduced by two symmetric, second-rank, tensor-valued internal state variables which represent the total area of open and closed micro-cracks contained within a representative material volume element.

Constitutive relations are formulated from basic principles of irreversible thermodynamics and continuum mechanics. It is shown that both mechanical compliances and thermal conductivities are affected by damage, and that the material symmetry is influenced by damage orientation.

The derivation of damage growth relations is motivated by meso-level fracture behavior. A specific example exhibits the dependence of damage growth on the detailed mechanical properties of matrix and fibrous materials and on the statistics of flaw positions and sizes. It is shown that mechanical loads tend to orient damage perpendicularly to the load direction, thereby introducing a degree of order to an initially random configuration.

20. DISTRIBUTION/AVAILABILITY OF ABSTRACT: UNCLASSIFIED/UNLIMITED ☒ SAME AS RPT. ☒ OTIC USERS ☒	21. ABSTRACT SECURITY CLASSIFICATION: unclassified
22a. NAME OF RESPONSIBLE INDIVIDUAL: Lt. Col. George Haritos	22b. TELEPHONE NUMBER (Include Area Code): (202) 767-0463; 22c. OFFICE SYMBOL: NA

DD FORM 1473, 83 APR — EDITION OF 1 JAN 73 IS OBSOLETE.

unclassified

SECURITY CLASSIFICATION OF THIS PAGE

A Damage Model for Uniaxially Reinforced Composites

by

Y. Weitsman

and

K. Lee

Final Scientific Report

to the

Air Force Office of Scientific Research

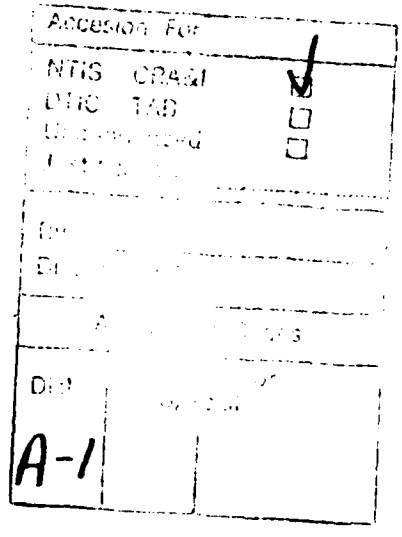

Research conducted under Grant

AFOSR-87-0128

March 1, 1987 - August 31, 1988

A DAMAGE MODEL FOR UNIAXIALLY REINFORCED COMPOSITES

Abstract

This report concerns a continuum damage model for uni-directionally reinforced composites that contain a multitude of micro cracks. Consideration is given to the coupling between mechanical and thermal effects. Damage is introduced by two symmetric, second-rank, tensor-valued internal state variables which represent the total area of open and closed micro-cracks contained within a representative material volume element.

Constitutive relations are formulated from basic principles of irreversible thermodynamics and continuum mechanics. It is shown that both mechanical compliances and thermal conductivities are affected by damage, and that the material symmetry is influenced by damage orientation.

The derivation of damage growth relations is motivated by meso-level fracture behavior. A specific example exhibits the dependence of damage growth on the detailed mechanical properties of matrix and fibrous materials and on the statistics of flaw positions and sizes. It is shown that mechanical loads tend to orient damage perpendicularly to the load direction, thereby introducing a degree of order to an initially random configuration.

1. INTRODUCTION

Continuum damage theory is a rapidly growing endeavor at the present time. A recent review [1], which contains a partial list of about fifty publications, is probably outdated already. Most applications concerned the response of concrete [2] and, to a somewhat lesser extent - of polycrystalline metals. In several recent papers the methodology of continuum damage was applied to fibrous and laminated composites[3]-[8]. Although a critical and comprehensive literature review goes beyond the scope of this report, the view taken here is that to be useful a damage theory must contain two essential ingredients:

(1) It should be amenable to rational development of damage growth relations ("kinetic" laws), and

(2) It should enable a comprehensive correlation between material properties, such as compliances and diffusivities, and damage.

It follows that "damage" should be endowed with an obvious physical meaning, because only under such circumstance it is possible to formulate rationally its growth and relationship with other physical quantities.

Typically, continuum damage theory applies to brittle materials which develop a profusion of micro-cracks prior to failure. It is then reasonable to associate "damage" with these micro-cracks - at least approximately. Approximations are necessary because a complete accounting for all micro-cracks poses an intractable and unsurmountable problem. In addition to the intricacies involved in solving the circumstance of a multi-cracked geometry in the presence of many inclusions, all realistic configurations of composite materials lack order and require statistical descriptions. It is therefore advisable to study damage in composites by highlighting its main features and ranking the relative importance of various factors, such as crack/crack and

crack/inclusion interactions, crack and inclusion spacings, etc. Such studies would lead to the construction of a useful continuum level damage theory with a quantitive understanding of the approximations involved therein.

In the present work, the construction of the damage parameters employed several approximations. These were: (i) on the micro-level, all damage was assumed to correspond to flat cracks, and (ii) on the macro-level, "damage" corresponded to the totality of micro-crack surfaces contained within a representative volume element.

The assumption of flat micro-cracks enabled the representation of their areas by vectors, say $\underline{D}$. However, since every crack possesses two equal and opposite areas, a representation which is invariant to the choice of any one of those two areas was given by the dyadic product $\underline{D}\,\underline{D}$. The macro-level assumption states that the damage variable is represented by $\underline{\underline{A}} = \Sigma\, \underline{D}\,\underline{D}$, hence by a symmetric second rank tensor. Upon division by an inherent material scale, e.g. the size of the representative volume, it is possible to construct the non-dimensional damage parameter $\underline{\underline{a}}$.

The micro-level assumption of flat cracks is mainly matter of mathematical expediency, which leads to the dyadic representation. The macro-level assumption involves a rather severe approximation, since it obliterates the distinction between small and large micro-cracks and disregards their relative spacings. Nevertheless, it will be suggested below that by allowing quantities like compliances to depend non-linearly on damage, it is possible to retain some measure of distinction between micro-level details. Furthermore, to account for thermal and diffusion processes it has been suggested to include a second continuum-level variable $\underline{\underline{c}}$, which represents the total area of closed ("passive") micro-cracks within the representative volume element. In the case of heat conduction, the heat generated through friction

occurs mostly at those passive surfaces while the process of molecular diffusion is most likely affected by the capillary paths available in the presence of $\underline{\underline{c}}$.

A qualitative tabulation of the roles of the active and passive damage parameters is shown below

Phenomenon	Active Cracks (parameter $\underline{a}$)	Passive Cracks (parameter $\underline{\underline{c}}$)
Mechanical Response	Important	Unimportant
Heat conduction	Unimportant	Important
Molecular Diffusion	Important	Important

Table 1: The roles of active and passive damage in various physical phenomena.

Turning to damage growth relations, the main thesis of this research has been that such mechanisms cannot be derived from macro-level theories. The basic reason for this argument is that damage growth is inherently a micro-level phenomenon which depends on meso-level geometric details. Consequently, the proposed approach is to solve, exactly or approximately, suitable meso-level boundary value problems and distill their essential features for incorporation in the coarser, continuum-level formulation. In this manner the statistical characteristics of the meso-level geometry will "filter" into the continuum model. An example for meso-level statistical effects on crack growth is provided in section 3 below.

In multi-phased composite materials, the presence of initial imperfections must be assumed as an inherent component of the material's structure. These flaws occur due to non-uniformities in the fiber positions which cause localizations in stress concentrations during the manufacturing process. In addition, flaws may be present due to nonuniformities in the

curing process, incomplete interfacial bondings or impurities. In glass/epoxy composites the positions of initial cracks correlated reasonably well with the locations of closest distances between adjacent fibers[9], where the residual stresses due to processing are highest. Since it is reasonable to assume that the energy necessary for crack initiation exceeds the energy required for crack growth, it follows that the major effect of external loads is to bring about the extension of the initial cracks rather than trigger new flaws. Consequently, the statistics of flaw location will remain, by and large, fixed, and only the flaw sizes (and shapes) will change under stresses. If the above hypothesis is correct then, once the statistics of initial flaws is prescribed, all crack interactions will depend mainly on $\underline{\underline{a}}$ (and perhaps $\underline{\underline{c}}$). Although the form of this dependence is unknown at the present time, the above hypothesis suggests that such dependence is likely to exist. For this reason, the continuum damage model developed herein retained a dependence of compliances and conductivities on functions of (the appropriate invariants of) $\underline{\underline{a}}$ and $\underline{\underline{c}}$ and a linearization in those parameters was deliberately avoided.

The representation of damage by symmetric, second-rank, tensor-valued parameters was employed by other investigators [10]-[14], to mention but a few, although their choices were derived from somewhat different physical considerations. In most of those cases damage was given by the symmetric tensor

$$d_{ij} = \frac{1}{2} \int_{S_c} ([u_i]n_j + [u_j]n_i)ds$$

where S_c denotes crack surface with normal $\underline{n}$ and $[u_i]$ expresses the jump in displacement across S_c.

The above choice is conceptually useful since d_{ij} expresses the contribution of the crack opening displacements to the softening of the material moduli. In principle d_{ij} can be related to the eigen strains e_{ij} associated with cracks. However, in actual computations any advantage of the above choice is diminished by the fact that expressions for e_{ij} are either very complicated or non-existent. Furthermore, in all current publications, effects of crack interactions are handled only through an iterative application of the self-consistent scheme. This scheme accounts for the moduli-softening effects of the surrounding cracks on the growth of a specific crack, but cannot handle the effects of inter-crack proximity or remoteness.

Regarding damage growth relations, some authors [11], [15] concurred with the premise that damage growth relations should derive from meso-level fracture behavior. However, no such mechanisms were thus far analyzed for composites. A rudimentary attempt to express damage growth in concrete was performed recently [15] (see also [16]), where a meso-level crack arrest mechanism within the aggregate/paste assemblage was described by an infinite-energy barrier spaced at some distance D which was related to the size of an aggregate's facet. Interactions among many cracks within an extended medium were considered only for homogeneous, isotropic materials[17]. No formulation exists at the present time for crack interactions in inhomogeneous materials.

2. THE DAMAGE MODEL

The detailed development of the model was given elsewhere [8]. For the sake of both clarity and brevity, we will provide in this section a two-dimensional version of the expressions listed in [8].

Fundamental considerations of continuum mechanics and irreversible thermodynamics yield the following expressions for energy balance and non-negative entropy production:

$$\rho_o \dot{\phi} = -q_{i,i} - \rho_o s \dot{T} - \rho_o T \dot{s} - \dot{\sigma}_{ij} \varepsilon_{ij} \tag{1}$$

and

$$-\rho_o \dot{\phi} - \rho_o s \dot{T} - \dot{\sigma}_{ij} \varepsilon_{ij} - (q_i/T) g_i \geq 0 \tag{2}$$

In eqns. (1) and (2), where infinitesimal deformation was assumed ($\varepsilon_{ij} \ll 1$), ρ_o denotes the constant mass density, s is entropy density, T is temperature, q_i and σ_{ij} are components of the heat-flux vector and the Cauchy stress-tensor, respectively, and ϕ is the Gibbs free energy, given by

$$\rho_o \phi = \rho_o u - \rho_o T s - \sigma_{ij} \varepsilon_{ij} \tag{3}$$

where u is the internal energy density.

Also, in eqns. (1) and (2), dot denotes derivative with respect to time and $g_i = \partial T/\partial x_i$ where x_i are Cartesian coordinates.

Assume a constitutive response given by

$$\phi = \phi(\sigma_{ij}, a_{ij}, c_{ij}, T)^* \tag{4}$$

where a_{ij} and c_{ij} are the active and passive damage variables described in section 1.

Since the inequality (2) cannot be violated for any process it follows that

$$\varepsilon_{ij} = -\rho_o \frac{\partial \phi}{\partial \sigma_{ij}} \tag{5}$$

$$s = -\frac{\partial \phi}{\partial T} \tag{6}$$

and

$$-\Gamma_{ij} \dot{a}_{ij} - \Pi_{ij} \dot{c}_{ij} - (q_i/T) g_i \geq 0 \tag{7}$$

*Familiar arguments rule out dependence of ϕ on g_i.

In eqn. (7) Γ_{ij} and Π_{ij} are the "affinities" given by

$$\Gamma_{ij} = \rho_o \frac{\partial \phi}{\partial a_{ij}}, \quad \Pi_{ij} = \rho_o \frac{\partial \phi}{\partial c_{ij}}$$

The above affinities can be interpreted as "macro level" energy release rates and energy dissipation rates associated with the growth of the total area of the active microcracks, and the closure of the passive flaws, contained within the RVE.

Substitution of eqns. (5) and (6) into eqn. (1) leads to the coupled heat conduction equation

$$-q_{k,k} = (\Gamma_{ij} - T \frac{\partial \Gamma_{ij}}{\partial T})\dot{a}_{ij} + (\Pi_{ij} - T \frac{\partial \Pi_{ij}}{\partial T})\dot{c}_{ij} + T \frac{\partial \varepsilon_{ij}}{\partial T} \dot{\sigma}_{ij} + \rho_o C \dot{T} \qquad (8)$$

In eqn. (8) $C = -T \frac{\partial^2 \phi}{\partial T^2}$ denotes specific heat at constant stress and damage.

Consider a uni-axially reinforced composite with all fibers parallel to the x_3 axis and all damage oriented in the x_1-x_2 plane (no cracks cutting across fibers), whereby $a_{13} = a_{23} = a_{33} = 0$. In addition, confine attention to the case of plane strain so that all dependencies on x_3 vanish. In this case, the expressions listed in [8] reduce to the following forms:

Two dimensional compliances:

$$\begin{aligned}
S_{11} &= 2L_2 + 2L_{22} + 2L_3(a_{11} - a_{22})^2 + 2L_{12}(a_{11} - a_{22}) \\
S_{12} &= 2L_2 - 2L_{22} - 2L_3(a_{11} - a_{22})^2 \\
S_{22} &= 2L_2 + 2L_{22} + 2L_3(a_{22} - a_{11})^2 + 2L_{12}(a_{22} - a_{11}) \qquad (9) \\
S_{26} &= 8L_3(a_{22} - a_{11})a_{12} + 4L_{12}a_{12} \\
S_{66} &= 2L_{22} + 32L_3 a_{12}^2
\end{aligned}$$

In the above L_2 and L_{22} are "classical" compliances while L_3 and L_{12} are "new", non-classical, terms.

Two-dimensional conductivities:

$$k_{11} = k_1 + k_3(a_{11} - a_{22})$$
$$k_{12} = 2k_3 a_{12} \qquad (10)$$
$$k_{22} = k_1 + k_3(a_{22} - a_{11})$$

where k_1 and k_3 are a "classical" and a "new" term, respectively.

Material symmetry considerations state that L_2, L_3, L_{12}, L_{22} as well as k_1 and k_3 may depend on <u>functions</u> of the transversely isotropic invariants of a_{ij} and c_{ij}. In two dimensions these invariants are:

$N_1 = a_{11}+a_{22}$, $N_2 = (a_{11} - a_{22})^2 + 4a_{12}^2$, $N_3 = c_{11}+c_{22}$, $N_4 = (c_{11}-c_{22})^2 + 4c_{12}^2$, and $N_5 = (a_{11}-a_{22})(c_{11}-c_{22}) + 4a_{12}c_{12}$.

The <u>specific</u> functional dependence of L_2, L_3, L_{12}, L_{22}, k_1, and k_3 on N_1, N_2, N_4, and N_5 cannot be inferred from continuum level formalisms or from symmetry requirements.

Note that damage induces changes in the material symmetry (through the "non-classical" quantities L_3, L_{12} and k_3) as well as affects the magnitudes of all compliances and diffusivities (through the invariants N_1 - N_5).

As noted earlier, linearization in a_{ij} and c_{ij} was deliberately avoided in eqns. (9) and (10). Such linearization would imply that a_{ij} and c_{ij} are infinitesimally small, thus restricting the model to sparse damage and discarding crack-interaction effects. It is worth noting that linearization was indeed performed in refs. [3]-[6].

To accentuate the coupling effects between damage and heat-conduction assume, for simplicity, that neither compliances nor diffusivities depend on temperature. Under this circumstance the coupled damage-heat-conduction equation reads:

$$\rho_o C \frac{\partial T}{\partial t} = -(k_{11} \frac{\partial^2 T}{\partial x_1^2} + 2k_{12} \frac{\partial^2 T}{\partial x_1 \partial x_2} + k_{22} \frac{\partial^2 T}{\partial x_2^2}) + D \qquad (11)$$

where the dissipation term D is given by

$$\begin{aligned} 2D = & (\frac{\partial S_{11}}{\partial a_{11}} \dot{a}_{11} + \frac{\partial S_{11}}{\partial c_{11}} \dot{c}_{11}) \sigma_1^2 + 2 (\frac{\partial S_{12}}{\partial a_{12}} \dot{a}_{12} + \frac{\partial S_{12}}{\partial c_{12}} \dot{c}_{12}) \sigma_1 \sigma_2 \\ & + (\frac{\partial S_{22}}{\partial a_{22}} \dot{a}_{22} + \frac{\partial S_{22}}{\partial c_{22}} \dot{c}_{22}) \sigma_2^2 \\ & + 2(\frac{\partial k_{11}}{\partial x_1} \frac{\partial T}{\partial x_1} + \frac{\partial k_{12}}{\partial x_1} \frac{\partial T}{\partial x_2} + \frac{\partial k_{12}}{\partial x_2} \frac{\partial T}{\partial x_1} + \frac{\partial k_{22}}{\partial x_2} \frac{\partial T}{\partial x_2}) \end{aligned} \qquad (12)$$

A specific expression for D requires a detailed knowledge of the dependence of all compliances and diffusivities on the damage invariants. Note also that terms like $\partial k_{11}/\partial x_1$ are expressible by the chain-rule as $(\partial k_{11}/\partial a_{11})(\partial a_{11}/\partial x_1) + (\partial k_{11}/\partial a_{12})(\partial a_{12}/\partial x_1) + \ldots$, etc.

3. DAMAGE GROWTH RELATIONS - An Illustration.

To demonstrate the correlation between meso-level fracture behavior and macro-level damage parameters consider the two dimensional case of interfacial debondings between fiber and matrix materials. Two drastic simplifying assumptions are employed: (i) all meso-level fracturing is confined to the fiber/matrix interfaces (namely - the critical energy release rate for debonding is smaller than the critical energies for all other failure mechanisms), and (ii) it suffices to consider a single crack-fiber-matrix system (namely the medium is sparsely reinforced and all other interactions are negligble).

Consequently, the problem is reduced to the consideration of a single arc crack growing along the interface between a single cylindrical inclusion and an extended homogeneous region, as shown in Fig. 1. The computations employed the analytical solution developed by Toya [18] which contains detailed expressions for stresses, displacements and energy release rates for the present problem.

A computational scheme was developed where, for given material properties, crack configuration, and external loads the energy release rates were evaluated by Toya's expression [Ref. 18, eqn. (4.7)] of the form

$$p^2 R\, F[\nu_1,\ \nu_2,\ \mu_1/\mu_2,\ \omega, \beta) = G \qquad (13)$$

In (13) p denotes the magnitude of the remote uniaxial tensile stress σ_x, ν_2 and μ_2 are the Poisson's ratio and shear modulus of the inclusion, ν_1 and μ_1 are the analogous values for the homogeneous exterior, and G is the energy release rate for interfacial debonding (combining modes I and II). Also, R denotes the radius of the inclusion, ω- the crack orientation and β half its arc size as shown in Fig. 1.

If for a given initial crack configuration G exceeds the critical value G_c, an iterative scheme is employed to determine values of ω and β that yield $G=G_c$. These values, $\omega = \omega_f$ and $\beta = \beta_f$, are subject to the requirement that no interpentration occurs along the crack surface. This requirement can be inferred from Toya's expression for the opening displacement [Ref. 8, Eqn. (3.57)], which takes the form

$$\Delta u_r = U(\nu_1,\ \nu_2,\ \mu_1/\mu_2,\ \beta,\ \omega) \qquad (14)$$

Obviously, if $\Delta u_r < 0$ anywhere along the arc crack described by ω_f and β_f, the latter values are inacceptable. Unfortunately, Toya's solution (and all other available solutions to this problem) fails whenever crack closure occurs. Such closures do in fact happen for interfacial cracks that are approximately parallel to the direction of a uni-axially applied tension. In the absence of an exact solution, an approximate iterative scheme was employed to handle cases of crack closure. The iteration proceeds as follows: (i) for a given crack geometry and an applied load the location of crack closure was

estimated from the condition $\Delta u_r = 0$, yielding values β^* and ω^* which fall within the range of the initial crack. (ii) Modifying the initial configuration to have one crack tip at β^* and ω^* employ eqn. (13), with $G=G_c$, to locate final crack positions β_f and ω_f (iii) check if and where according to eqn. (14) $\Delta u_r = 0$ within the final crack positions that were evaluated by the previous step. (iv) Repeat iterations until β^*, ω^* and β_f, ω_f converge.

Similarly, for sufficiently small loads, when $G < G_c$, closure may occur over portions of a stationary initial crack. In such cases too, employment of the condition $\Delta u_r = 0$ as prescribed by eqn. (14) provides an estimate of the closed portion. If $\Delta u_r > 0$ over the entire stationary initial crack, then it is fully open.

Note that the above procedure gives inexact results, because it treats the contact region as a perfectly re-welded crack, albeit with compressive normal stresses. In the absence of a better alternative, this approximation is employed in the present work.

To focus attention on statistical aspects, it was assumed that cracks may occur with equal probability anywhere along the boundary r=R of the inclusion and that their size was normally distributed, rather tightly, about a mean value.

In our computations we employed values similar to those of Toya [18], namely: $\mu_1 = 0.346$ msi, $\nu_1 = 0.35$, $\mu_2 = 6.41$ msi, $\nu_2 = 0.22$, and $R = 0.19 \times 10^{-3}$ in. Although not stated explicitely in ref. [18], it was implied therein that $G_c = 0.284 \times 10^{-5}$ in.-lb./in.

The distribution of crack sizes was assumed Gaussian ("Normal"), with a mean half-arc angle of 5° and a standard deviation of 0.5°. The positions around the circumference were assumed to be uniformly distributed.

The number of crack-fiber samples, N, within a hypothetical representative volume element was taken as N=40 and N=80 to assess the sensitivity of the results to this parameter. The magnitude of the remote load was varied from 100 to 3000 psi in steps of 100 psi. No further crack growth at the fiber/matrix interfaces occurred for $\sigma > 3000$ psi.

The variation and distributions of crack sizes with load are shown in Figs. 2(a), (b), (c), (d) for four random sets of initial cracks with N=40 and in Fig. 2(e) for N=80. The differences between the results shown in Figs. 2(a)-(d) are due to the different realizations in the initial values of the random variables ω and β that occurred in those sets of samples. These realizations were selected through a computer-aided random number generator (Program "IMSL").

The most interesting feature to emerge from Figs. 2(a)-2(e) is that under increasing loads crack growth divides into four distinct categories. These categories are denoted by A,B,C, and D, with typical configurations sketched within Figs. 2(a)-2(e). The percentage of cracks within each category is indicated by the lengths of the vertical bars drawn above curves A,B,C, and D.

Cracks in category A remain inert to the load $\sigma_x = p$. For sufficiently small loads, when no growth occurs, this category contains all cracks. Note that some of the A-cracks contain closed ("passive") segments, of magnitudes indicated by the shaded parts of the vertical bars.

Curves marked with the letter B give the <u>average</u> size of cracks where the far tips remain stationary and whose entire growths were caused by their near tips growing towards the line-of-action of the remote load.

Curves C correspond to a fixed magnitude (half arc angle) of $\beta_f = 57.3°$ and orientation $\omega_f = 0$, namely all cracks in this category are aligned

symmetrically about the load's line-of-action. It can be noted that as the load increases higher percentages of initial cracks snap into the configuration of category C. Note that cracks in this category are entirely open and that configuration C is reached by growth at both remote and near crack-tips.

Finally, cracks in category D correspond to final configurations which nearly circumscribe the entire fiber/matrix interface. For any given value of remote load all the cracks in this category have the same final geometrical shape, although - unlike in category C - this shape varies with the load. Cracks in category D are symmetric about the load's line-of-action, with open and closed segments as sketched within Figs. 2(a)-2(e). The percentage of the closed ("passive") portions can be inferred from the shaded portions of the vertical bars above curves D.

It should be noted that all the closed portions of the cracks (in categories A and D) occur along segments that are farthest from the line of action of the applied load. The statistical scatter among the results shown in Figs. 2(a) -2(e) is demonstrated by the histograms exhibited in Fig. 2(f).

The re-orientation of the micro-cracks about the load line-of-action, ω, is shown in Figs. 3(a), (b), (c), and (d) for N = 40 and in Fig. 3 (e) for N = 80 for increasing load amplitudes. Since this effect is even in the angle ω, the plotted results treated cracks centered at $(-\omega)$ as equivalent to those centered about the angle ω itself. In Figs. 3(a)-3(e) the results for categories A,B,C,D are shown separately and distinction is made between angles ω_c for the closed cracks and ω_a for the open cracks. Note that since all cracks in category C, and all the active cracks in category D, are oriented at $\omega = 0$ for all load levels, their plots coincide with the horizonal axes in figs. 3(a) - (e).

The strong influence of loading on the size and orientation of the microcracks is further demonstrated by the phase diagrams shown in figs. 4(a),(b), and (c).

In Figure 4(a), trajectories of average size and average location of the active and passive cracks in category A are shown under increasing loads, for five randomly selected distributions of initial cracks. Values at distinct load levels are marked off by various symbols, and trends under increasing loads are noted by arrows along the trajectories. Open symbols correspond to active cracks and closed symbols to passive cracks. Note that, with increasing loads, all active-crack values converge to a common location while the passive cracks retain their statistically dispersed character. However, in view of figs. 2(a)-2(e), and as will be seen in Fig.5, the comparative sizes of all cracks in Category A are very small and their contributions to the damage parameters as loads increase can be neglected.

Figs. 4(b) and 4(c) provide phase diagrams for the sizes and positions of the active and passive microcracks in Category D under increasing load levels. As noted earlier, in this category both size and position do not depend on the statistics of the initial microcracks. The arrows in Figs, 4(b) and 4(c) point the direction of the trajectories under increasing load.

Figures 5(a) - 5(e) give values of the continuum-damage parameters a_{xx}, c_{xx}, and c_{yy} with increasing loads. Values of a_{yy}, a_{xy}, and c_{xy} are omitted since they turned out to be negligibly small. These figures also show the contributions of the microcracks in categories C and D to the total values of a_{xx}, c_{xx}, and c_{yy}. Note that as the load increases, the micro-cracks in categories C and D dominate the entire damage phenomenon. In fact, comparisons among Figs. 5(a) through 5(e) show that the statistics of initial flaws has a much stonger influence on the damage parameters than does the retention of the complete listing of micro-crack categories.

4. CONCLUSIONS

A continuum damage model was formulated for uni-axially reinforced composites with two tensor-valued damage variables, a_{ij} and c_{ij}, that corresponded to the totality of open and closed micro-crack surfaces contained within a representative volume element. Following the basic premises of continuum damage, it was hypothesized here that all the essential features of damage-affected material response can be described - to within a reasonable approximation - with the variables a_{ij} and c_{ij}.

It has been argued that damage growth relations should be derived from meso-level fracture mechanics solutions. These detailed results should be then re-cast in terms of the fewer macro-level, continuum variables and parameters. Statistical aspects of meso-level micro-structure should also be reflected in the continuum level predictions.

The development of damage growth relations was demonstrated by means of an idealized example. In that example all micro-cracks were assumed to be confined to the fiber/matrix interfaces, and all interactions with other cracks and fibers were discarded.

The above example showed that under increasing external load initially disordered micro-cracks grow into orderly patterns, forming arrays that can indeed be described by fewer damage parameters. Specifically, it is shown in Figs. 5(a)-5(e) that to attain a very satisfactory approximation it sufficed to focus attention on two highly ordered crack configurations. These figures showed that sample to sample variations caused by the random nature of the initial flaws affected a scatter in the values of the damage parameters which was much larger than the contributions of the unpatterned cracks in categories

A and B. This indicated that the approximation inherent in describing the actual multi-cracking process by means of the macro-level damage parameters a_{ij} and c_{ij} is pragmatically useful.

Although much more work must be done to address the more realistic cases of cracks that deviate from the fiber/matrix interfaces and incorporate the effects of crack interactions, the present report indicates that the proposed continuum damage model possesses the essential features which are necessary to describe the damage process.

Acknowlegements

We wish to thank Professors E. Parzen and N. Stubbs of Texas A&M University for helpful discussions and suggestions concerning the st tistical aspects contained in this report.

References

[1] D. Krajcinovic: "Continuum Damage Mechanics". In "Applied Mechanics Update" (C.R. Steele and G.S. Springer - Editors). ASME, pp. 397-406 (1986).

[2] Z.P. Bazant: "Mechanics of Distributed Cracking". App. Mech. Rev. Vol. 39, No. 5 pp 675-705 (1986).

[3] R. Talreja: "A Continuum Mechanics Characterization of Damage in Composite Materials", Proceedings of the Royal Society London, Vol. A399, pp. 195-216, (1985).

[4] R. Talreja: "Stiffness Properties of Composite Laminates With Matrix Cracking and Interior Delamination", Engineering Fracture Mechanics, Vols. 5-6, pp. 751-762, (1986).

[5] R. Talreja: "Modeling of Damage Development in Composites Using Internal Variables Concepts". In "Damage Mechanics of Composites" (A.S.D. Wang and G.K. Haritos - Editors) ASME Pub. AD-Vol. 12, pp. 11-16 (1987).

[6] D.H. Allen, S.E. Groves and C.E. Harris: "A Thermomechanical Constitutive Theory For Elastic Composites With Distributed Damage. Part I: Theoretical Development ", To appear in International Journal of Solids and Structures, (1987).

[7] Y. Weitsman: "Coupled Damage and Moisture Transport in Fiber-Reinforced Polymeric Composites". International Journal of Solids and Structures Vol. 23, No. 7, pp. 1003-1025 (1987).

[8] Y. Weitsman: "Damage Coupled with Heat Conduction in Uni-axially Reinforced Composites". Journal of Applied Mechanics ASME - forthcoming. (= Report MM 5662-87-19, Grant AFOSR-87-0218, Dec. 1987).

[9] T. Seni and M. Bader. Private communication of a forthcoming paper.

[10] M. Kachanov: "Continuum Model of Medium with Cracks," Journal of the Engineering Mechanics Division," ASCE, vol. 106, no. EM5, pp. 1039-1051 (1980).

[11] M. Kachanov: "On Modelling of Anisotropic Damage in Elastic Brittle Materials - A Brief Review". In "Damage Mechanics in Composites" (A.S.D. Wang and G.K. Haritos - Editor). AD-Vol. 12, ASME. Dec. 1987, pp. 99-105.

[12] Murakami, S. and Ohno, N., 1981, "A Continuum Theory of Creep and Creep Damage." In "Creep in Structures." International Union of Theoretical and Applied Mechanics, 3rd Symposium, Leicester, UK, September 8-12, 1980. (A.R.S. Ponter and D.R. Hayhurst - Editors) Springer-Verlag, pp. 422-444.

[13] L.G. Margolin: "Elastic Moduli of a Cracked Body". Int. J. Fracture Vol. 22, pp. 65-79 (1983).

[14] D. Fanella and D. Krajcinovic: "A Micromechanical Model for Concrete in Compression". Eng. Fracture Mech., Vol. 29, No. 1 pp. 49-66 (1988).

[15] D. Krajcinovic and D. Sumarac: "Micromechanics of the Damage Processes". In "Continuum Damage Mechanics Theory and Applications" (CISM Courses and Lectures No. 295). (D. Krajcinovic and J. Lemaitre - Editors). Springer-verlag 1987, pp. 135-194.

[16] D. Krajcinovic: "Micromechanics of Concrete". Final report to AFOSR (S.Wu - Program Manager). January 1988.

[17] M. Kachanov: "Elastic Solids with Many Cracks: A Simple Method of Analysis". International Journal of Solids and Structures, Vol. 23, No. 1, pp. 23-43 (1987).

[18] M. Toya: 1974, "A Crack Along the Interface of a Circular Inclusion Embedded in an Infinite Solid". Journal of the Mechanics and Physics of Solids, Vol. 22, pp. 325-348.

Figure Titles

Fig. 1: A crack at the interface of a cylindrical inclusion and an extended exterior region ($r = R$, $\omega - \beta < \theta < \omega + \beta$), which is subjected to a remote uniaxial tension $\sigma_x = p$.

Figs. 2(a), (b), (c), (d): Crack sizes β (degrees) vs. load p (psi) for four randomly selected distributions of initial flaws. Number of sample members N = 40. Cracks divide into four categories A, B, C, and D as sketched in insert. (In those sketches, arc between arrows corresponds to the initial crack and locations of active and passive final cracks are also outlined). Percentage of cracks in each category indicated by lengths of vertical bars above curves. Shaded portion corresponds to passive cracks. Curves A and B provide average values of β. Curves C and D provide common β values.

Fig. 2(e): Same as Figs. 2(a) - 2(d), but N = 80.

Fig. 2(f): Histograms of crack angles β in categories A,B,C, and D at five selected values of the applied load, exhibiting the average values and the scatter among Figs. 2(a)-2(e).

Figs. 3(a), (b), (c), (d): Crack orientation ω (degrees) vs. load p (psi) for four randomly selected distributions of initial flaws with N = 40. ——— corresponds to the active cracks in category A, — — — to the passive cracks in category A, — — — to category B, and —·—·—· to the passive cracks in category D. Note that for all loads $\omega = o$ for all cracks in category C and for the active cracks in category D.

Fig. 3(e): Same as figs. 3(a)-3(d), but N = 80.

Fig. 4(a): Phase diagram showing trajectories for the average size β and average orientation ω of cracks in category A under increasing loads. Active portions with open symbols and passive portions with filled symbols. The five pairs of curves correspond to five random selections of inital cracks. Symbols ● ○ correspond to N = 80. All others to N = 40. Trends with increasing loads indicated by arrows. Angles in degrees.

Fig. 4(b): Phase diagram for the active portion of cracks in category D under increasing loads. Direction of trajectory indicated by arrow. Note that trajectory reverses sense at $\beta = 25.35^\circ$ and $\omega = 0.0246^\circ$.

Fig. 4(c): Phase diagram for the passive portion of cracks in category D under increasing loads. Direction of trajectory indicated by arrow.

Figs. 5 (a), (b), (c), (d): Components of damage variables (All magnitudes relative. Not scaled by size of RVE). Vs. load, corresponding to four randomly chosen samples of initial cracks, with N = 40.

Curve 1 gives c_{xx} due to cracks in category D.

Curve 2 gives c_{xx} due to cracks in all categories.

Curve 3 gives c_{yy} due to cracks in category D.

Curve 4 gives c_{yy} due to cracks in all categories.

Curve 5 gives a_{xx} due to cracks in category C.

Curve 6 gives a_{xx} due to cracks in category D.

Curve 7 gives the combined values of a_{xx} due to cracks in both C and D categories.

Curve 8 gives a_{xx} due to all categories.

Fig. 5(e): Same as Figs. 5(a) - 5(d), but with N = 80.

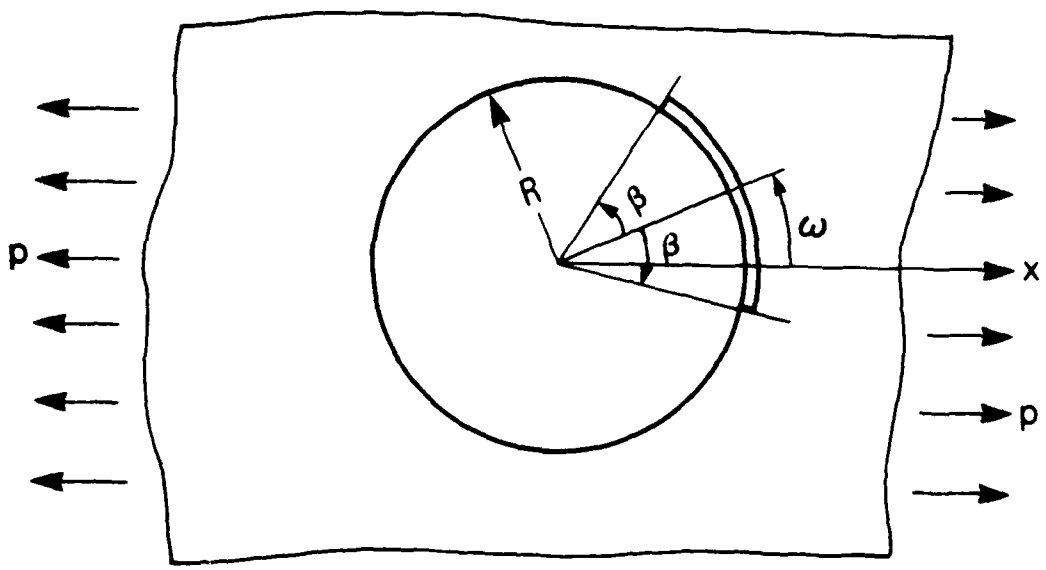

Fig. 1

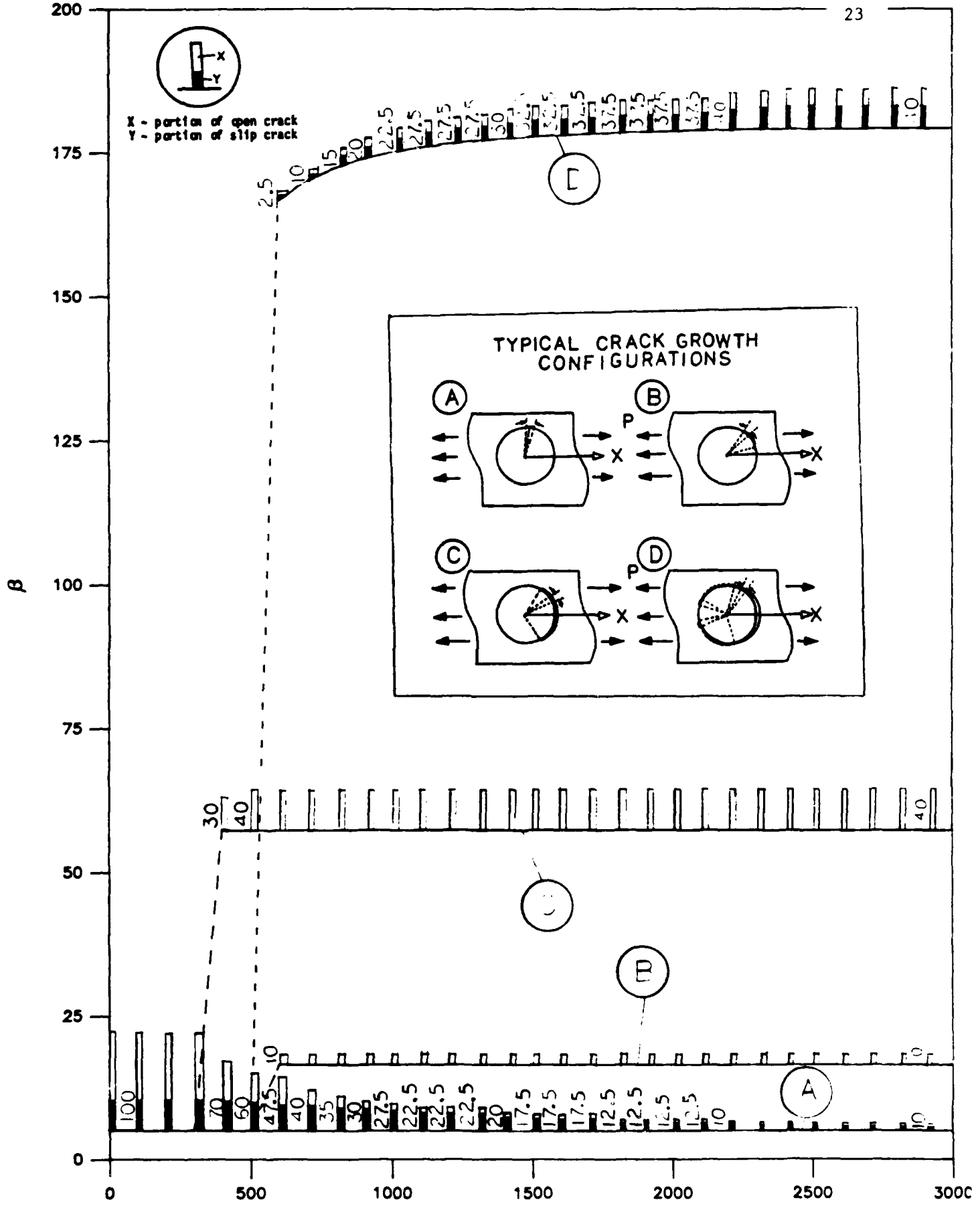
X - portion of open crack
Y - portion of slip crack
TYPICAL CRACK GROWTH CONFIGURATIONS
A
B
C
D
P
X
β
0
25
50
75
100
125
150
175
200
0
500
1000
1500
2000
2500
3000

Fig. 2(a)

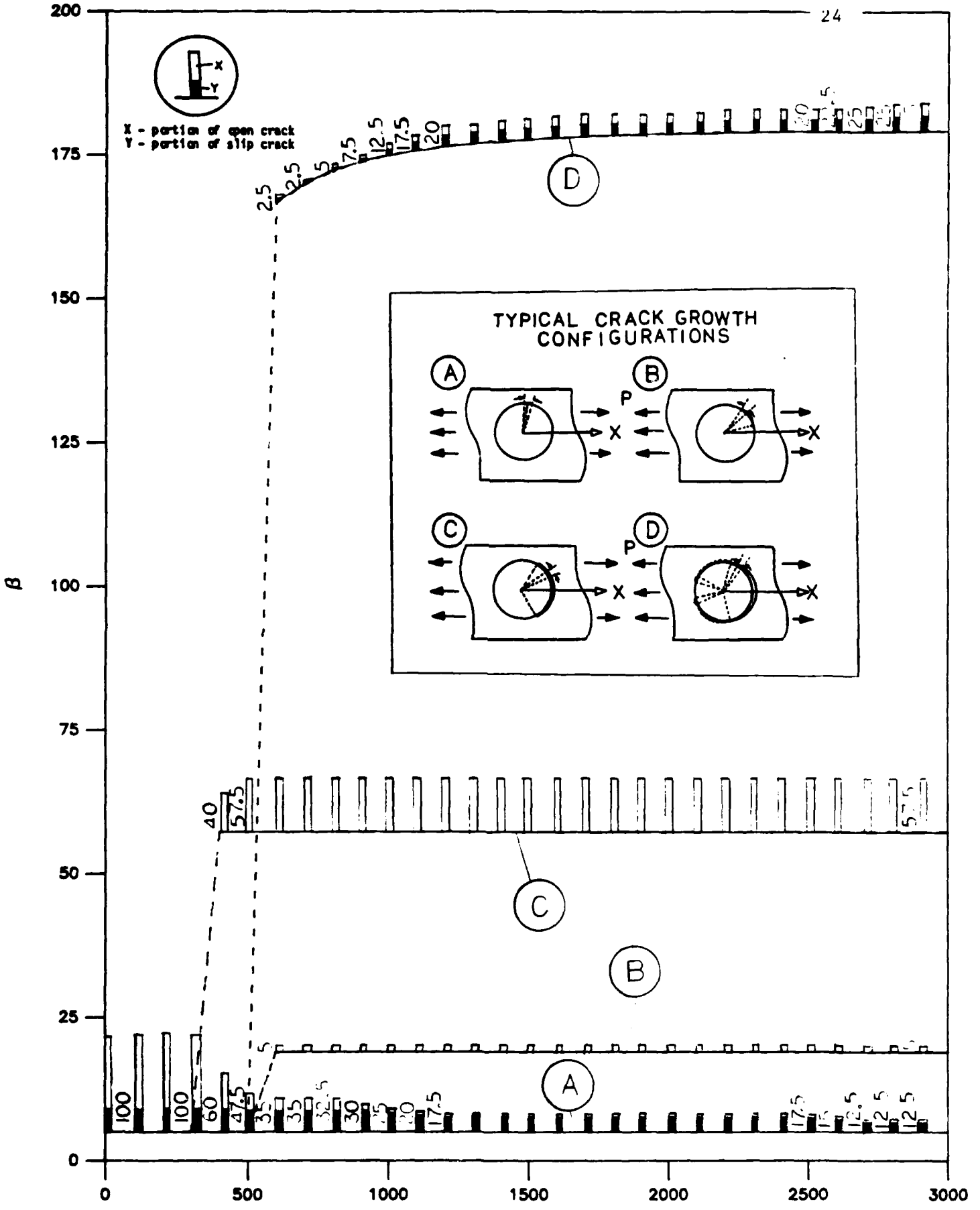
X - portion of open crack
Y - portion of slip crack
TYPICAL CRACK GROWTH CONFIGURATIONS
A
B
C
D
P
X
β
0
25
50
75
100
125
150
175
200
0
500
1000
1500
2000
2500
3000

Fig. 2(b) P

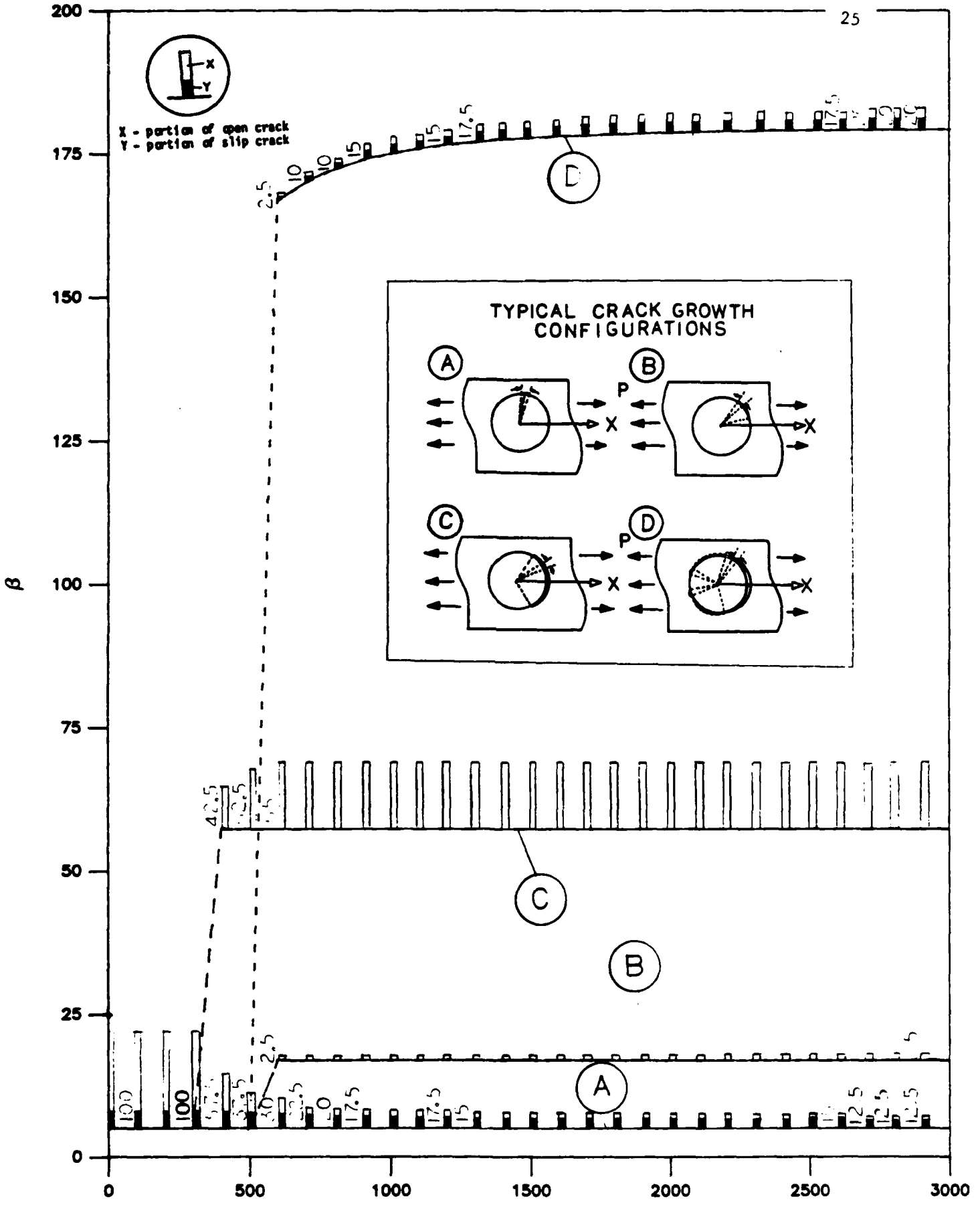
X - portion of open crack
Y - portion of slip crack
TYPICAL CRACK GROWTH CONFIGURATIONS
A
B
C
D
P
X
β
P
0
25
50
75
100
125
150
175
200
0
500
1000
1500
2000
2500
3000

Fig. 2(c)

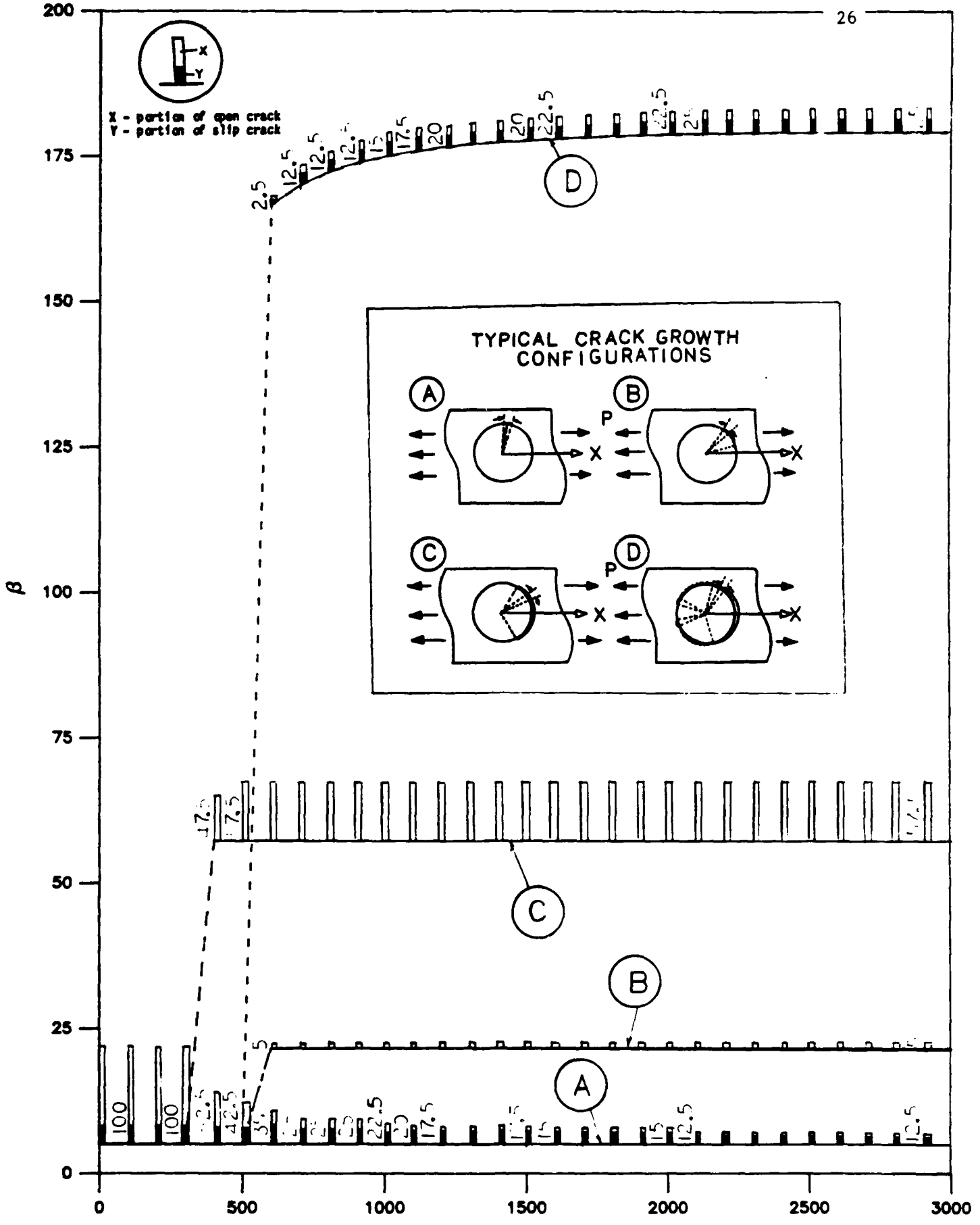
X - portion of open crack
Y - portion of slip crack
TYPICAL CRACK GROWTH CONFIGURATIONS
A
B
C
D
P
X
β
P
0
25
50
75
100
125
150
175
200
0
500
1000
1500
2000
2500
3000

Fig. 2(d)

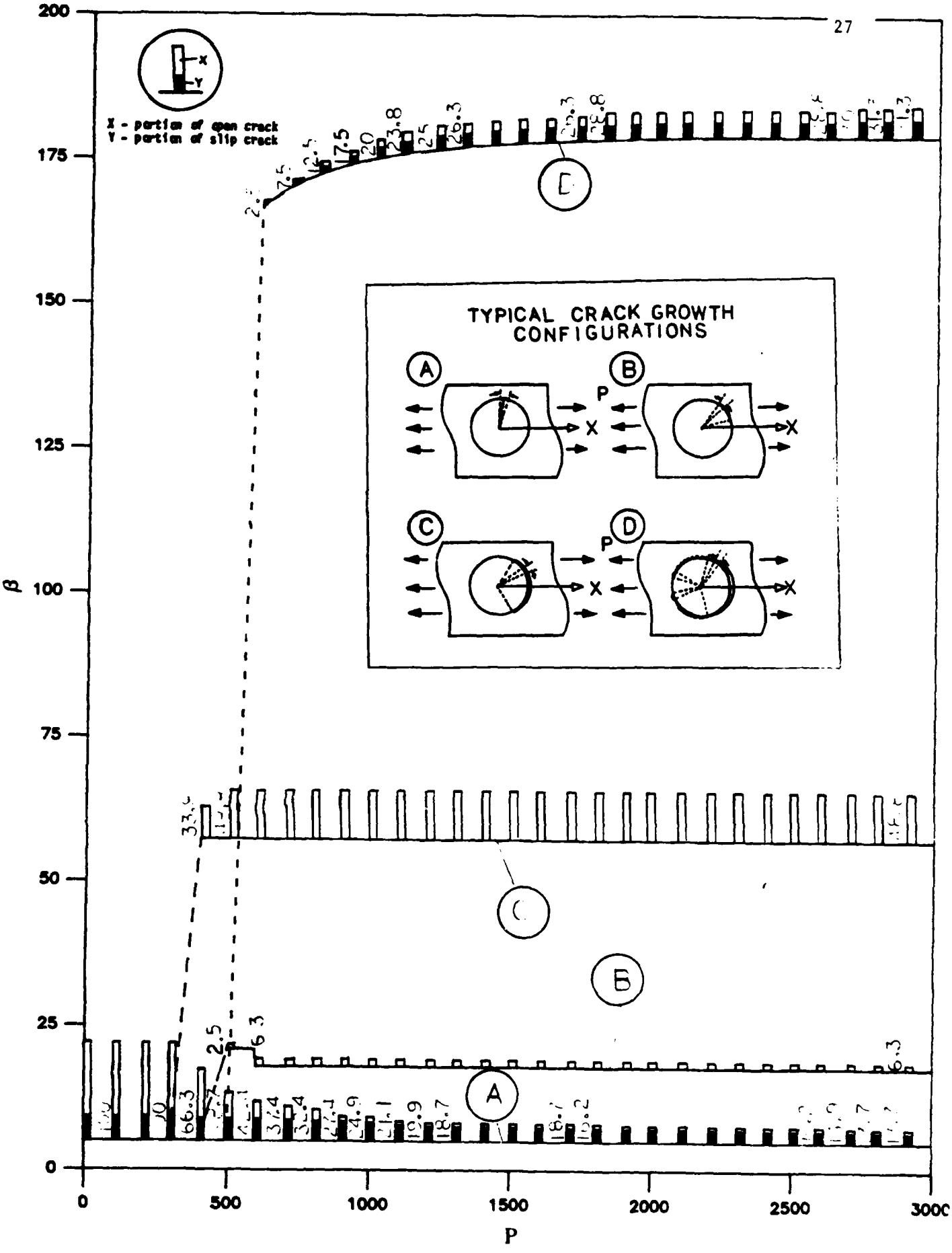
X - portion of open crack
Y - portion of slip crack
TYPICAL CRACK GROWTH CONFIGURATIONS
A
B
C
D
P
X
β
P
0
25
50
75
100
125
150
175
200
0
500
1000
1500
2000
2500
3000

Fig. 2(e)

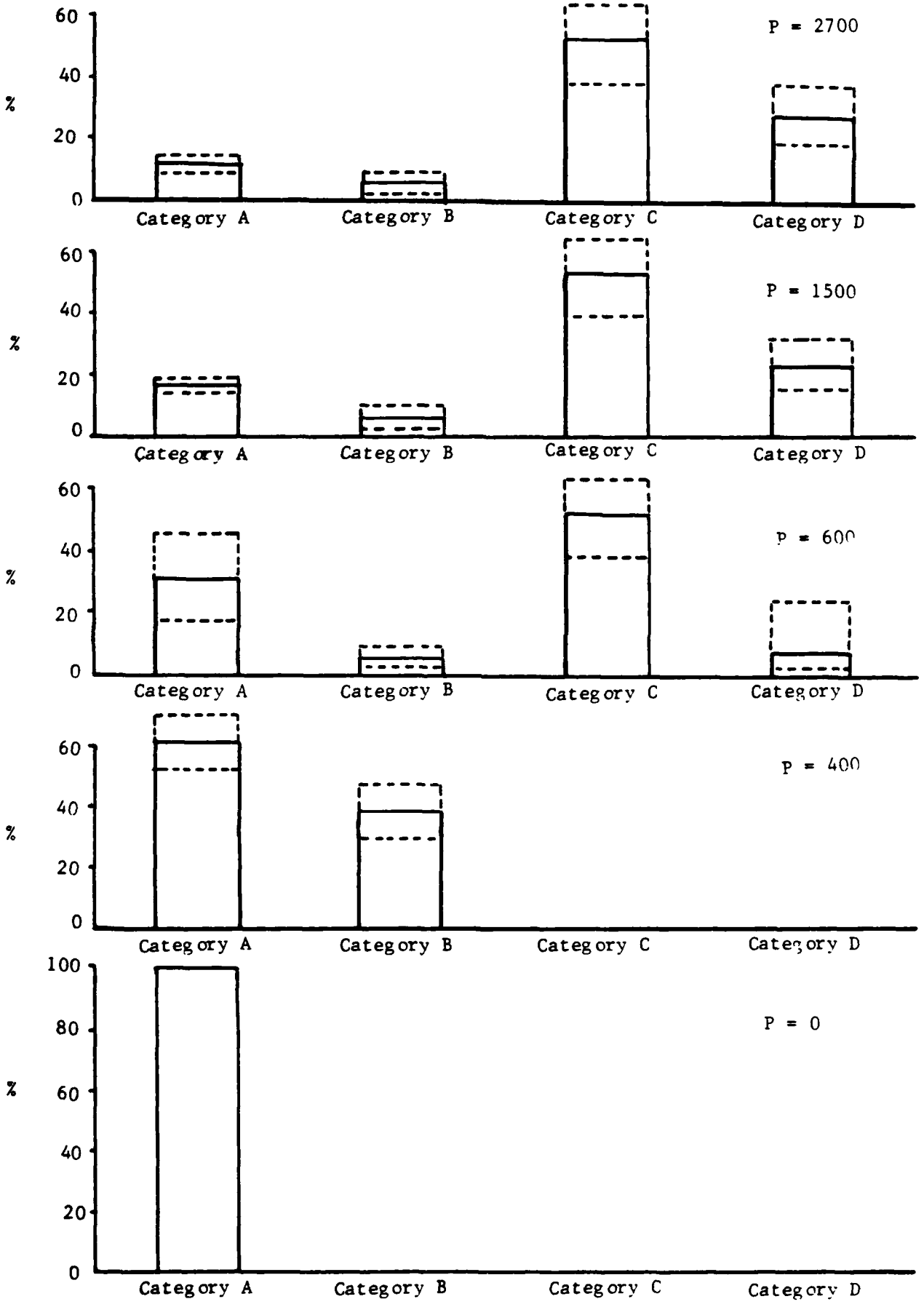
60
40
%
20
0
P = 2700
Category A
Category B
Category C
Category D
60
40
%
20
0
P = 1500
Category A
Category B
Category C
Category D
60
40
%
20
0
P = 600
Category A
Category B
Category C
Category D
60
40
%
20
0
P = 400
Category A
Category B
Category C
Category D
100
80
%
60
40
20
0
P = 0
Category A
Category B
Category C
Category D

Fig. 2(f)

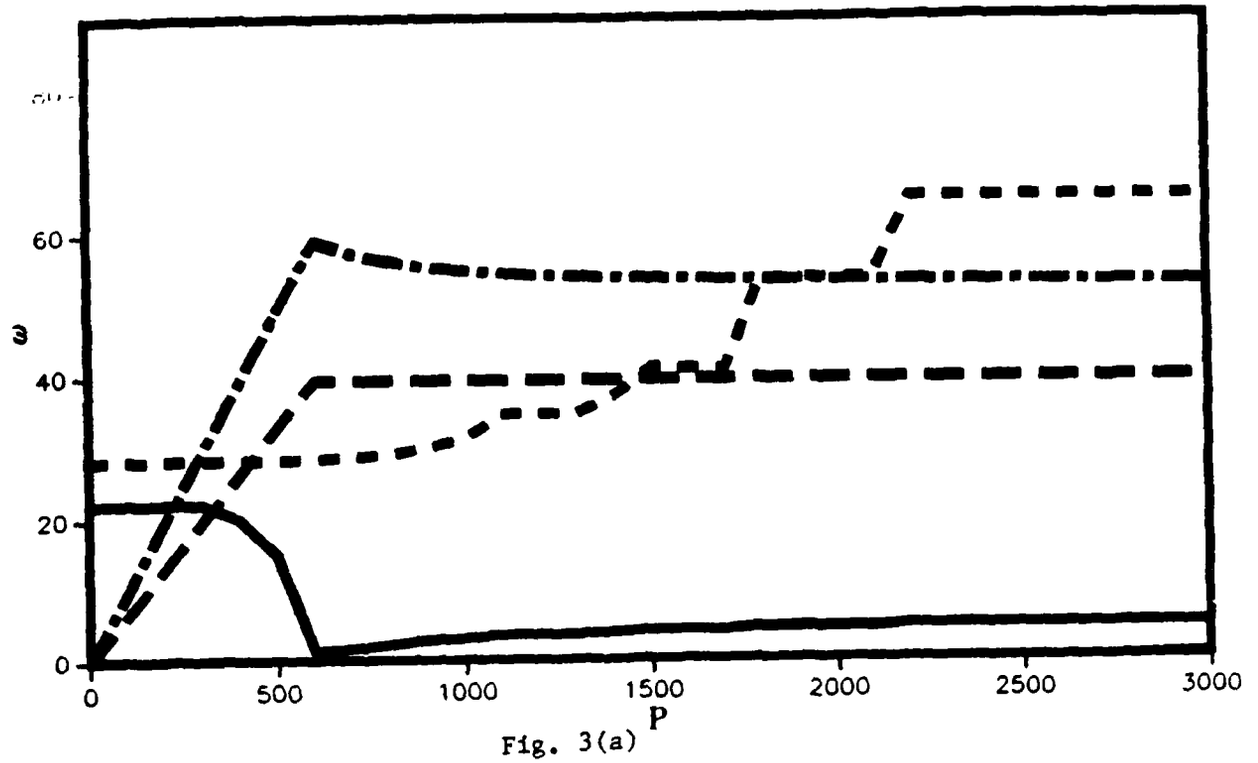
60
40
20
0
0
500
1000
1500
2000
2500
3000
P

Fig. 3(a)

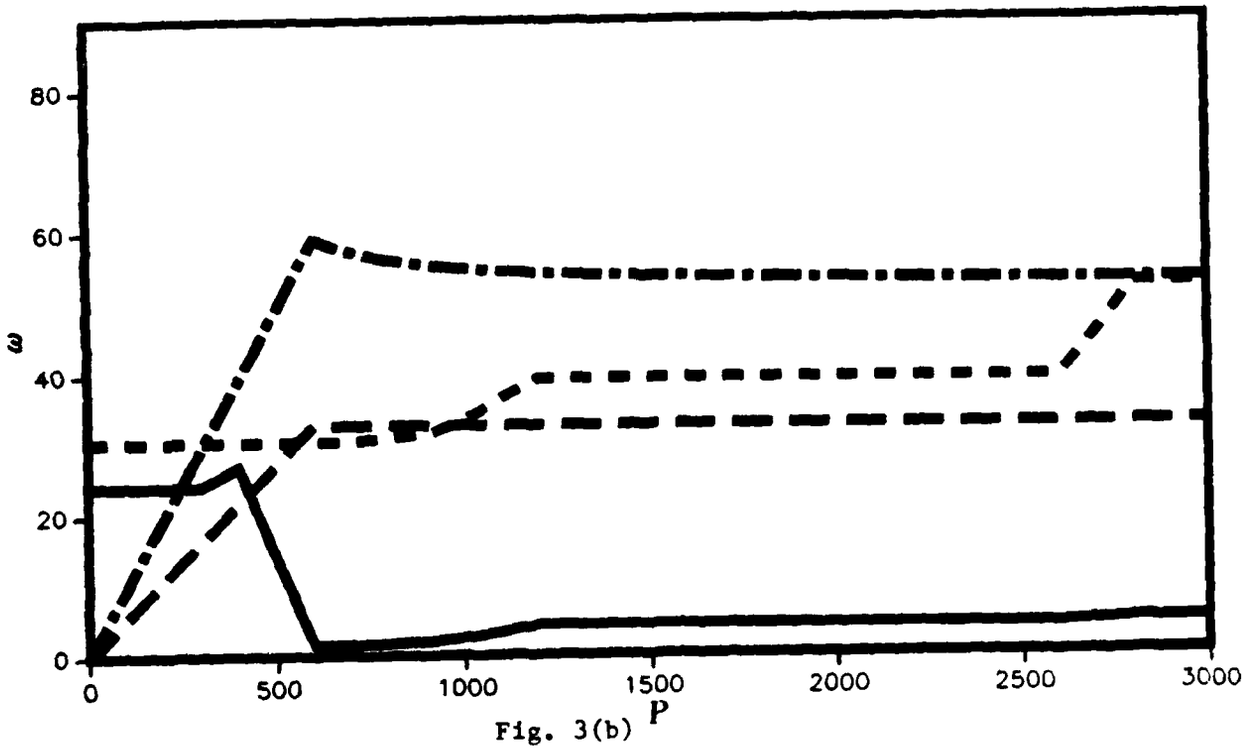
80
60
40
20
0
0
500
1000
1500
2000
2500
3000
P

Fig. 3(b)

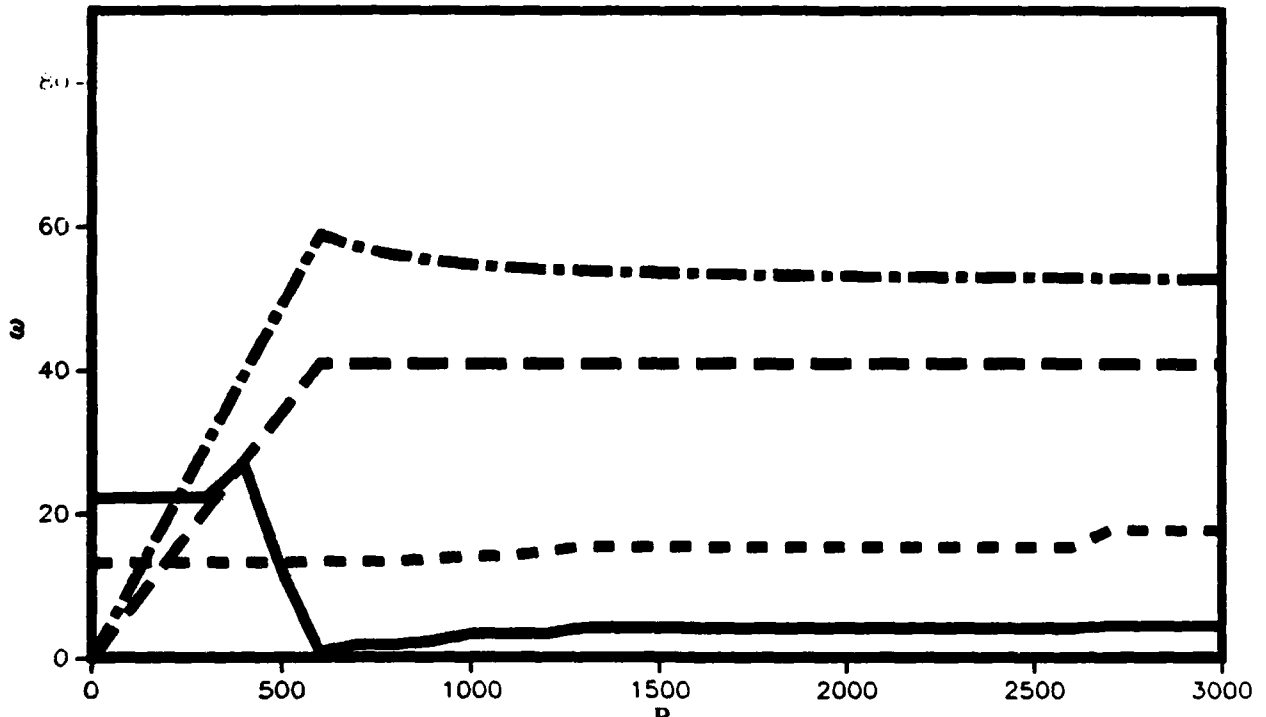
80
60
40
20
0
0
500
1000
1500
2000
2500
3000
P

Fig. 3(c)

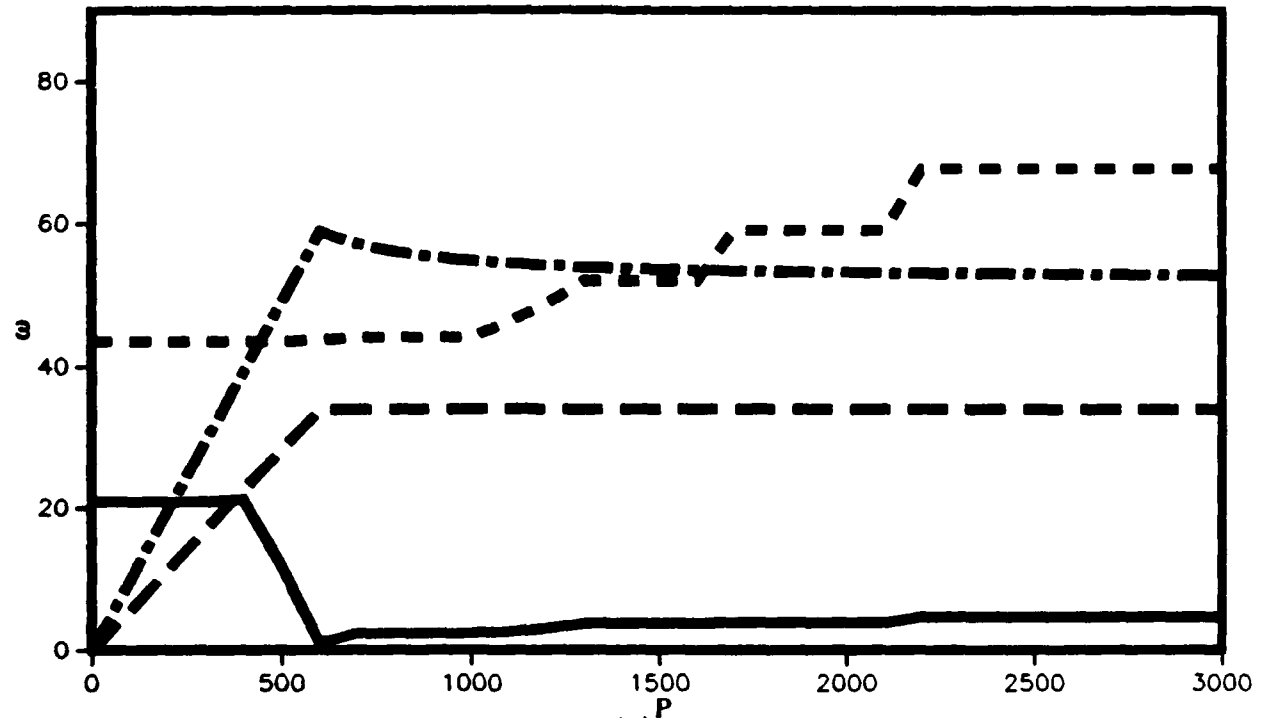
80
60
40
20
0
0
500
1000
1500
2000
2500
3000
P

Fig. 3(d)

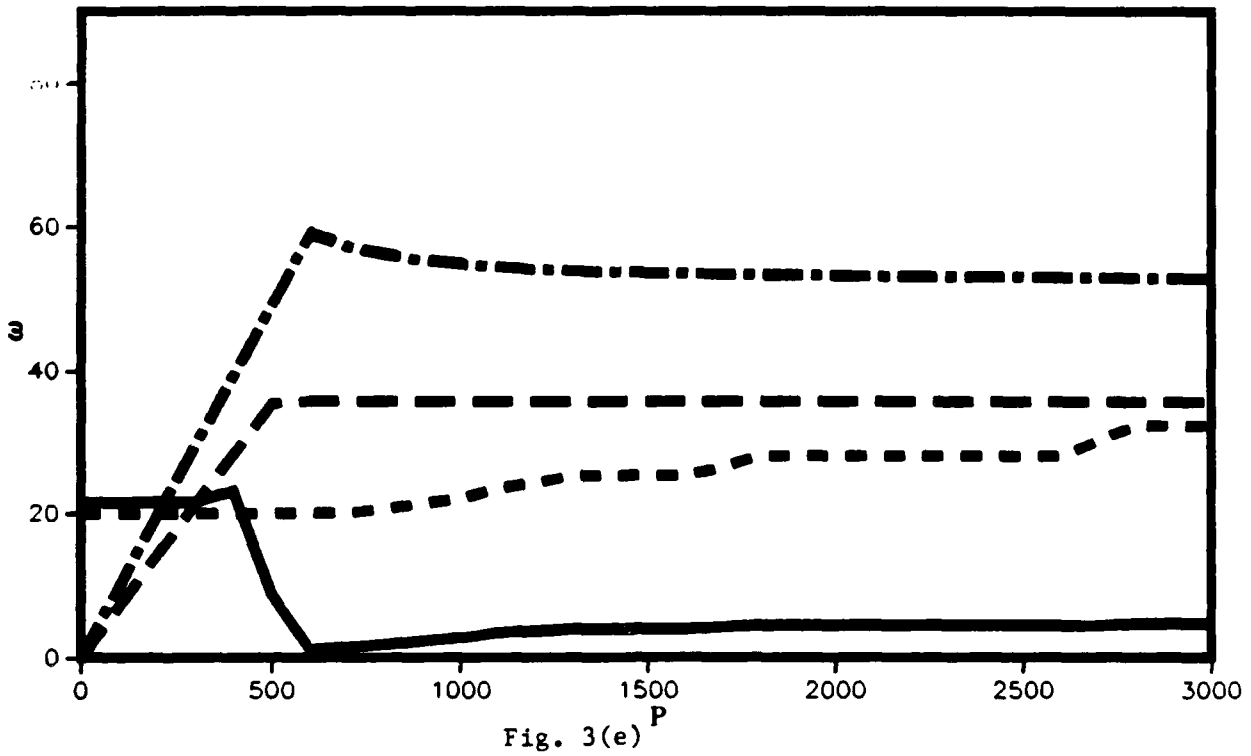

Fig. 3(e)

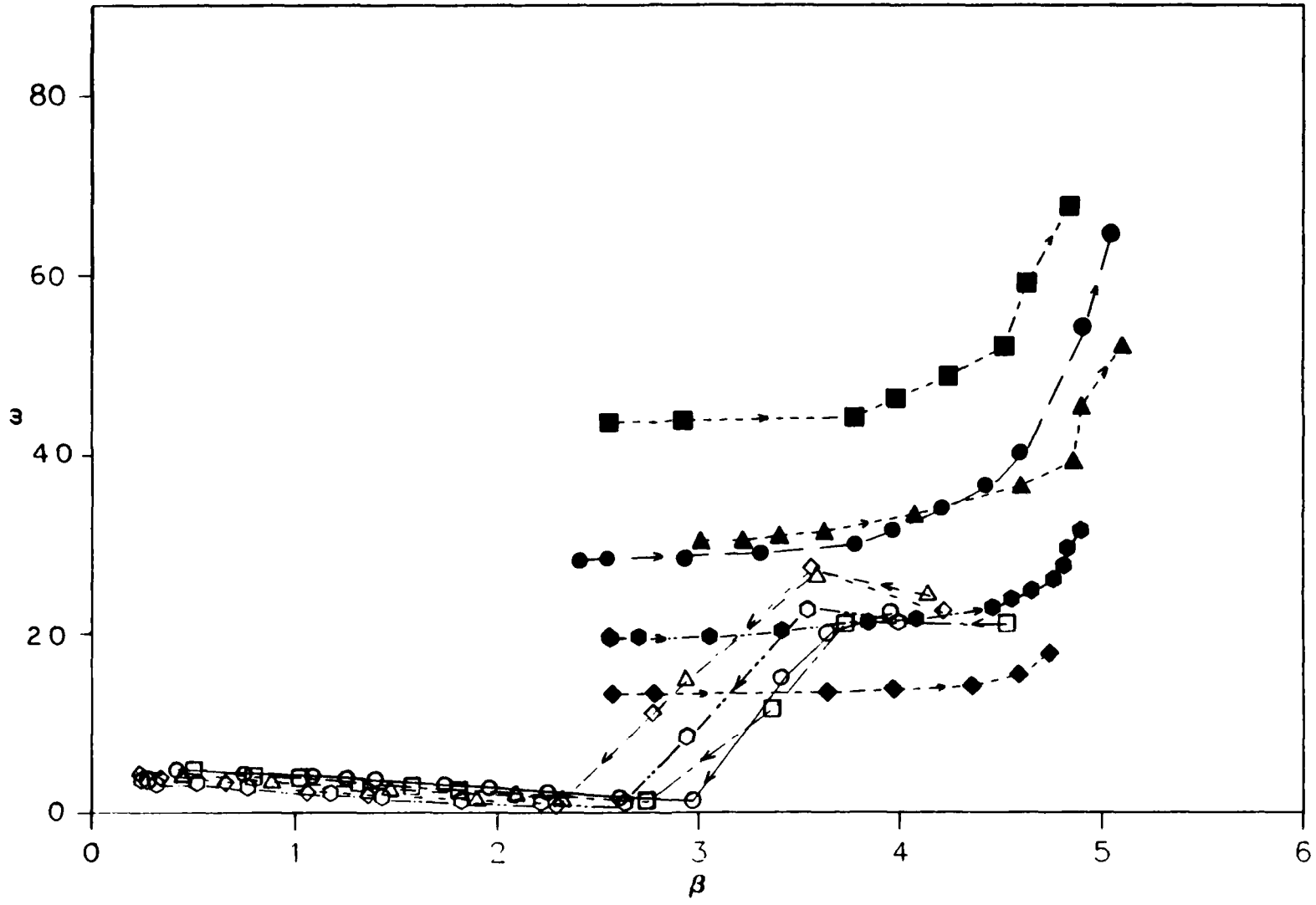

Fig. 4(a)

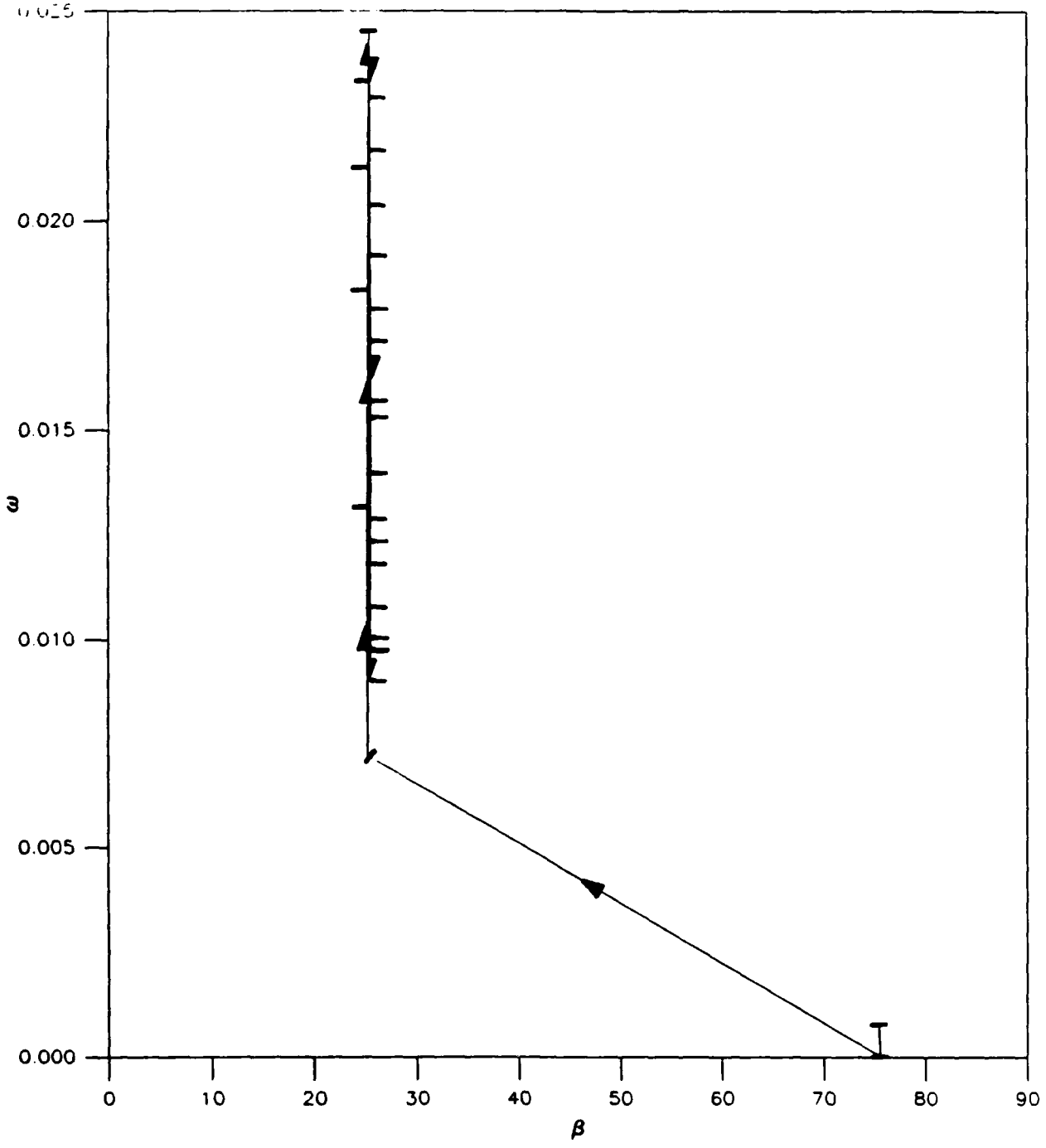

Fig. 4(b)

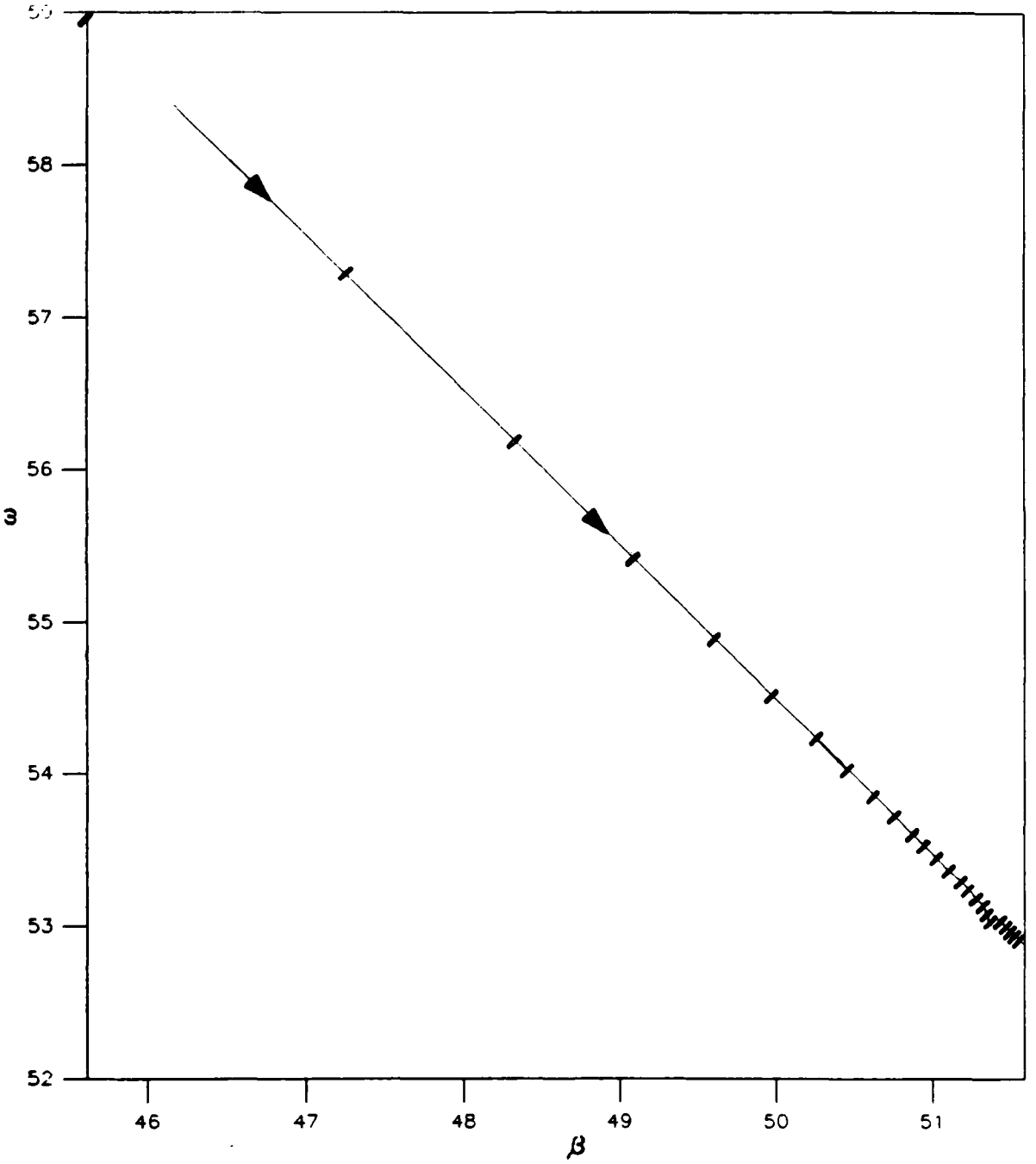

Fig. 4(c)

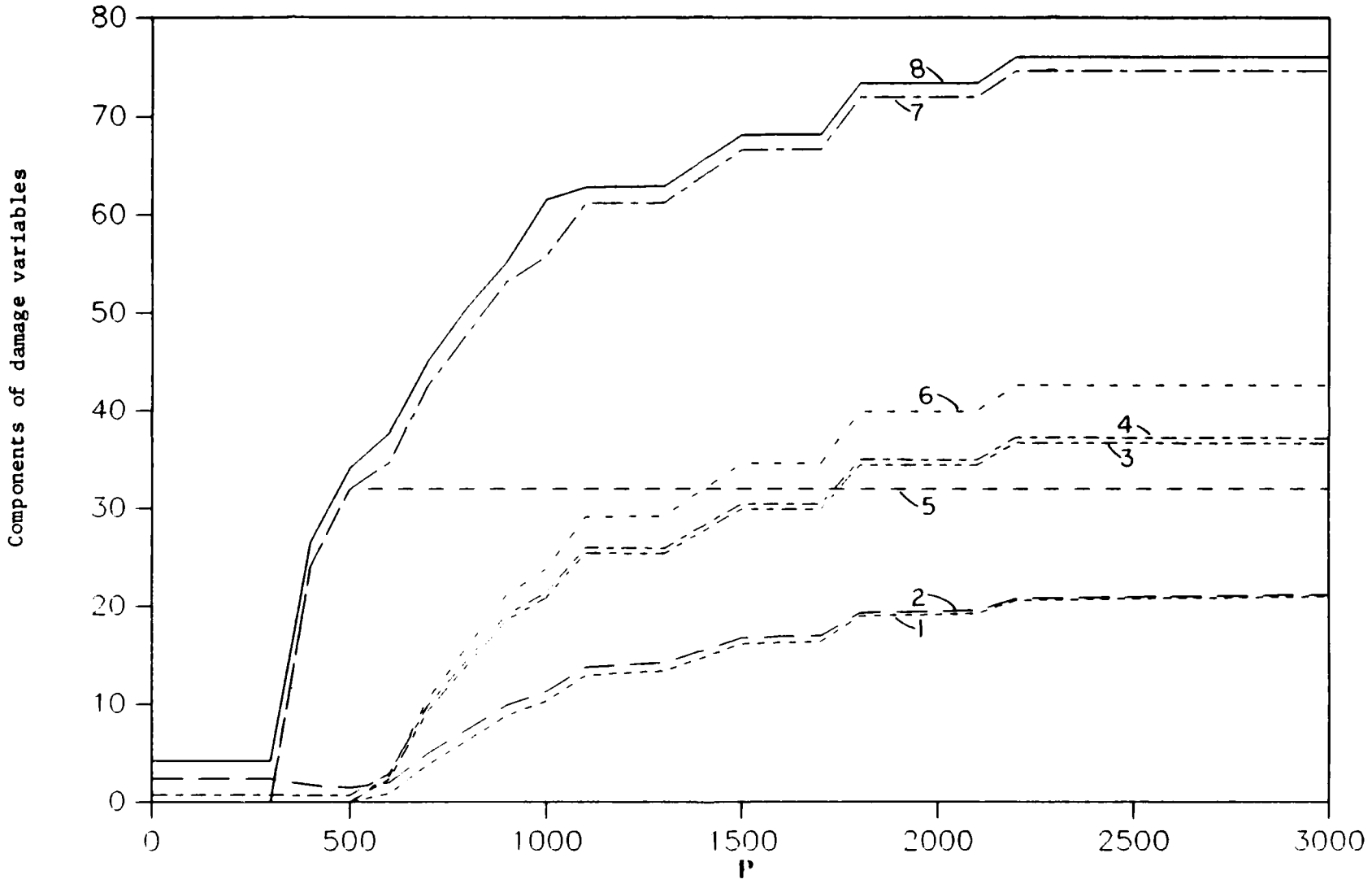
Components of damage variables
80
70
60
50
40
30
20
10
0
0
500
1000
1500
2000
2500
3000
P
8
7
6
4
3
5
2
1

Fig. 5(a)

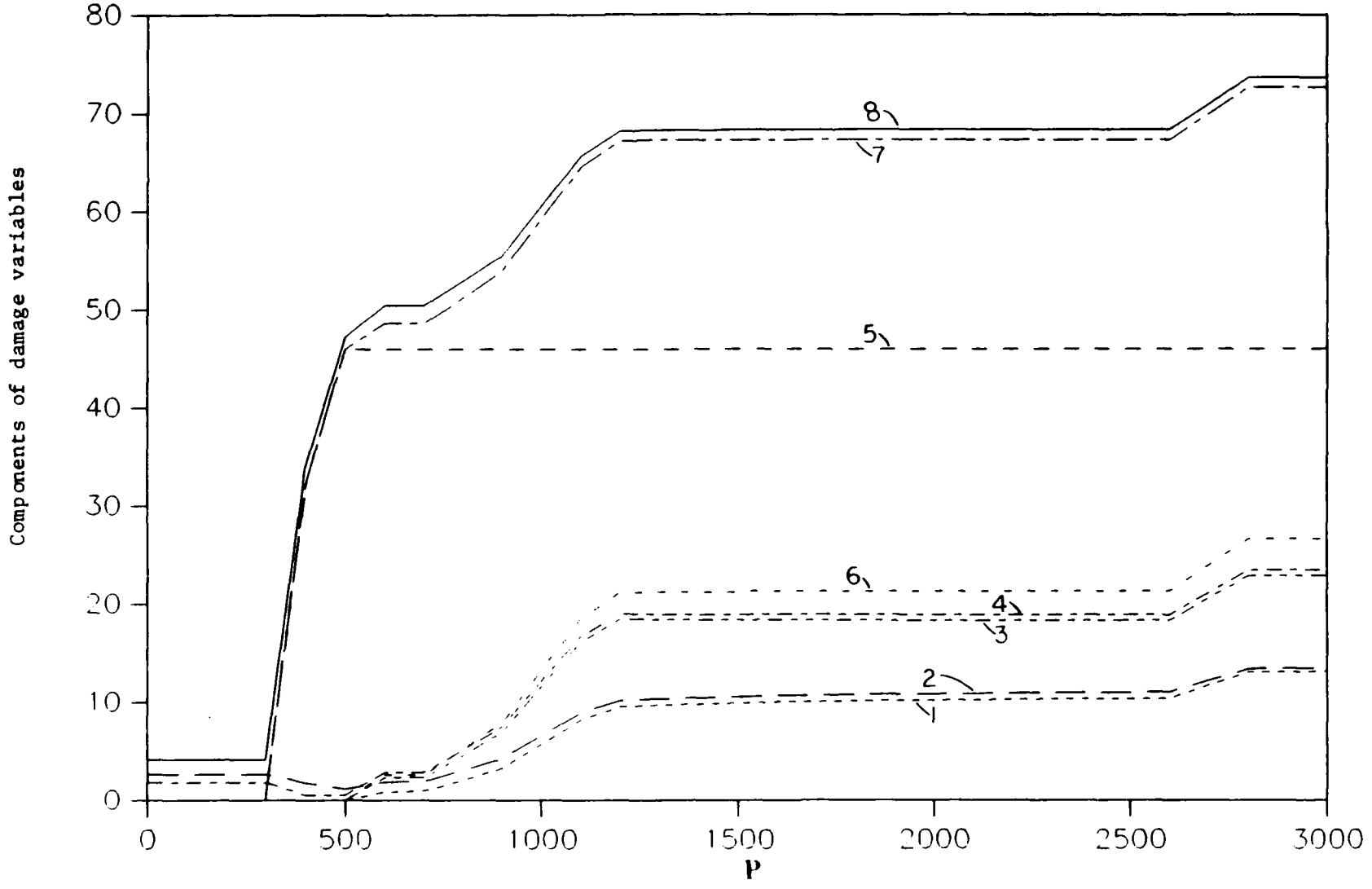
Components of damage variables
80
70
60
50
40
30
20
10
0
0
500
1000
1500
2000
2500
3000
P
8
7
5
6
4
3
2
1

Fig. 5(b)

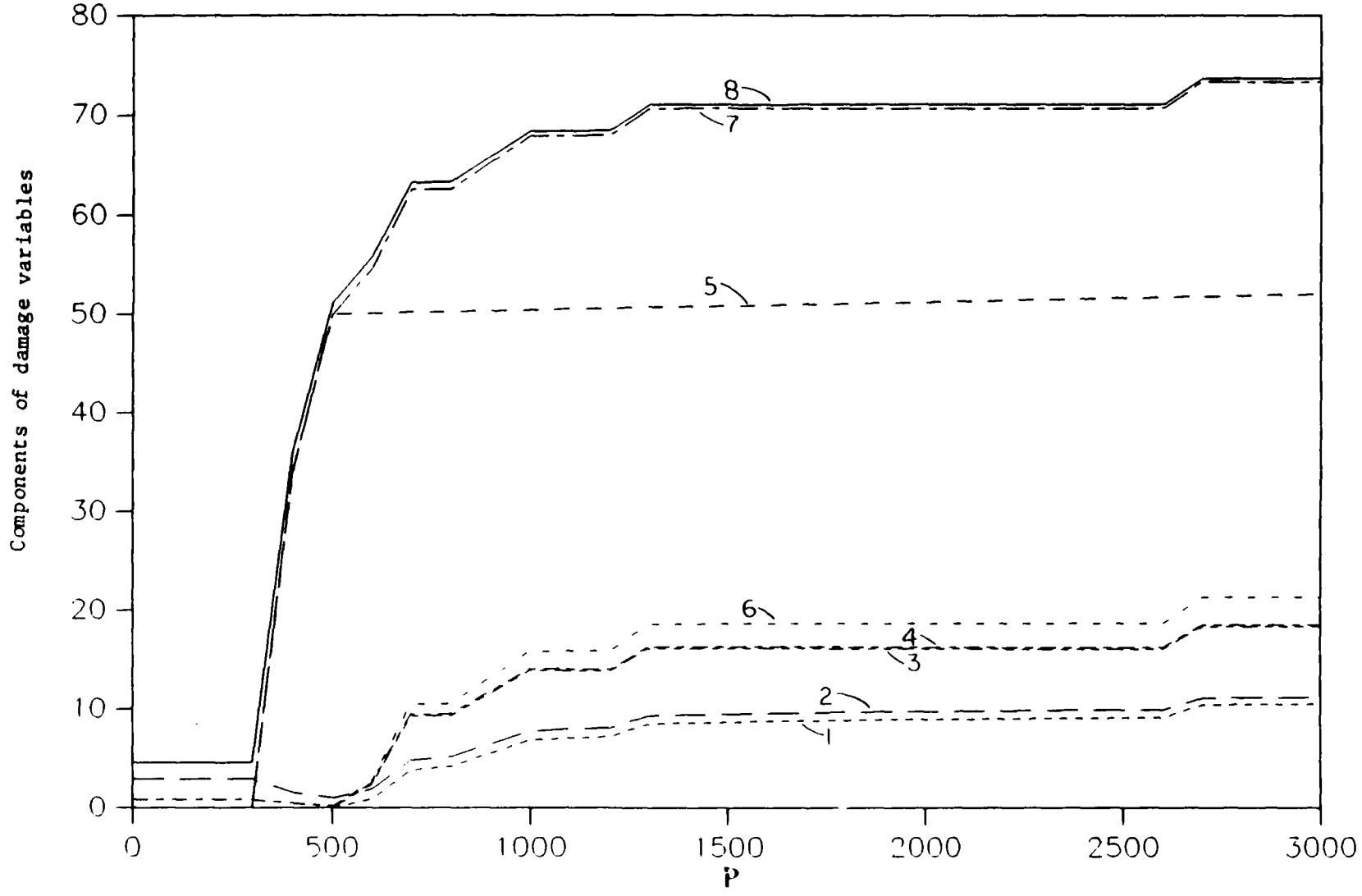
Components of damage variables
80
70
60
50
40
30
20
10
0
0
500
1000
1500
2000
2500
3000
P
8
7
5
6
4
3
2
1

Fig. 5(c)

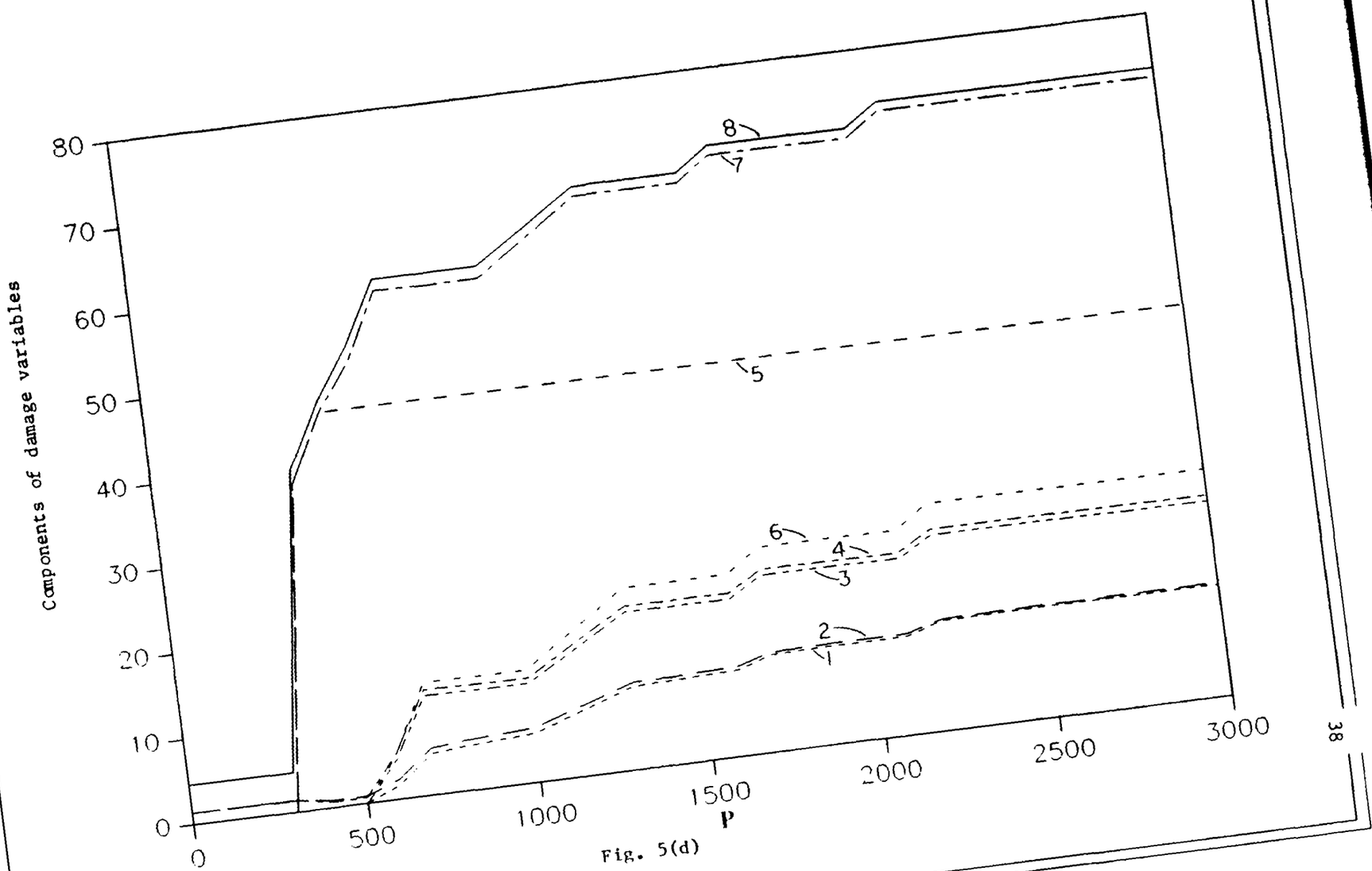
Components of damage variables
80
70
60
50
40
30
20
10
0
0
500
1000
1500
2000
2500
3000
P
8
7
5
6
4
3
2
1

Fig. 5(d)

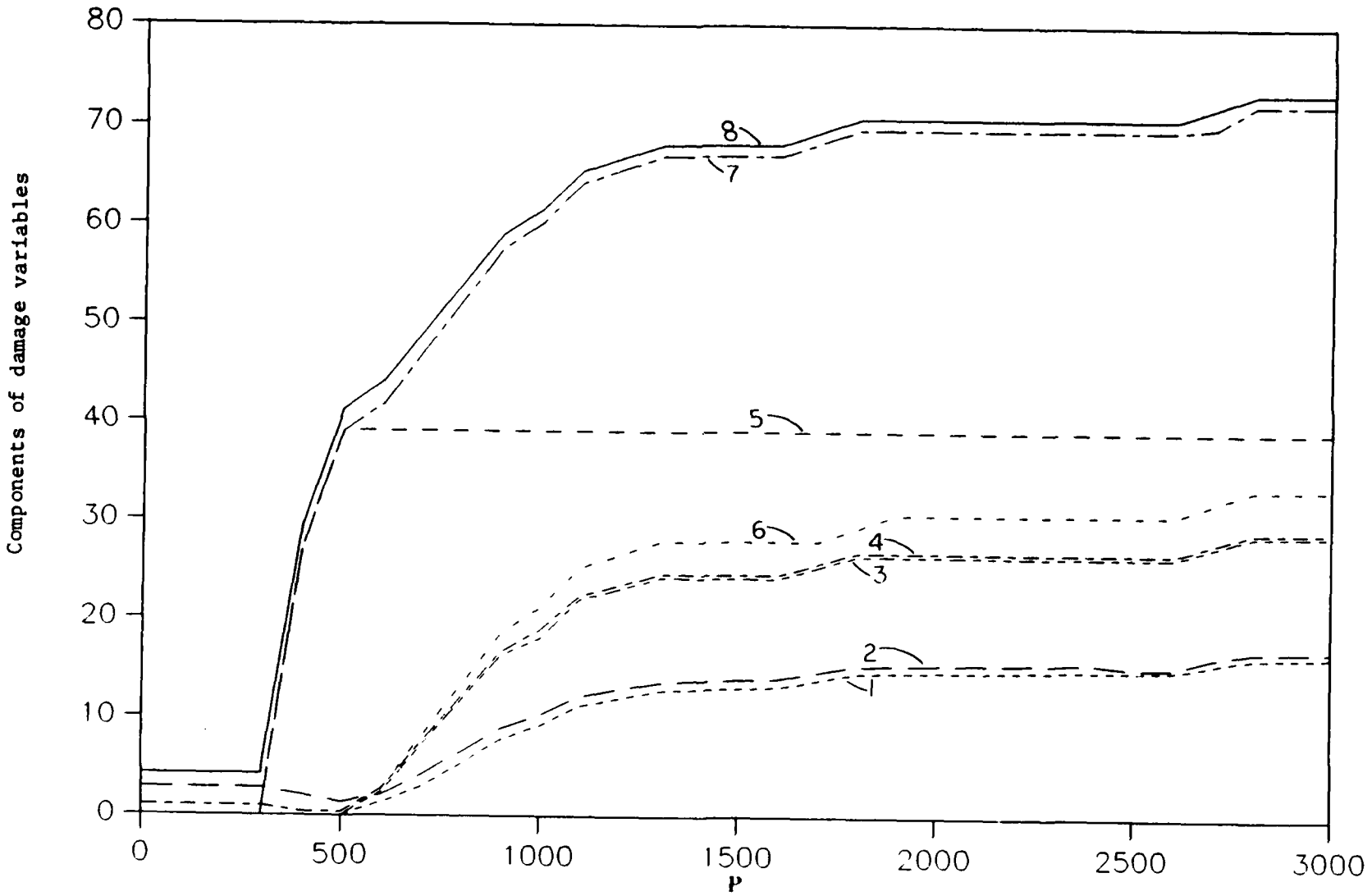
Components of damage variables
80
70
60
50
40
30
20
10
0
0
500
1000
1500
2000
2500
3000
P
8
7
5
6
4
3
2
1

Fig. 5(e)